Smart traffic manager for speed harmonisation and stop-and-go waves mitigation dedicated to connected autonomous vehicles

Léa Prade Njoua Dongmo, Jean Auriol, Alessio Iovine

Smart traffic manager for speed harmonisation and stop-and-go waves mitigation dedicated to connected autonomous vehicles

Léa Prade Njoua Dongmo, Jean Auriol, *Member IEEE*, Alessio Iovine, *Member IEEE*

***Abstract*—The present paper introduces a smart traffic manager, conceived as an algorithm tasked with supervising vehicles. It gathers and disseminates macroscopic traffic flow data among Connected Autonomous Vehicles (CAVs) to facilitate their attainment of string stability. This method combines machine learning techniques and physics-based traffic flow models, establishing a crucial connection between microscopic and macroscopic modeling levels. It enables CAVs to utilize mesoscopic controllers that effectively mitigate stop-and-go waves while ensuring speed harmonization, thereby proving their disturbance string stability. Simulation results demonstrate the efficacy of this proposed solution.**

***Index Terms*—Stop-and-go mitigation, string stability, microscopic traffic control, macroscopic traffic control, mesoscopic controllers, mixed ODE-PDE control systems, freeway traffic congestion.**

I. Introduction

THE advancement of cutting-edge traffic management technologies, allowing vehicles to adjust their behavior based on real-time traffic conditions, constitutes a significant topic nowadays since it implies minimizing the frequency and severity of traffic congestion, accidents, and gridlocks [1], [2], [3]. Due to the new possibilities provided by the development of intelligent infrastructures, Connected Autonomous Vehicles (CAVs) using Vehicle-to-Infrastructure (V2I) and Vehicle-to-Vehicle (V2V) communication technologies are a reality in smart transportation [4], which categorizes them in the Vehicle-to-Everything family (V2X).

In the present paper, we consider V2I technologies to empower CAVs to establish seamless communication with roadside infrastructure, thus showing how they play a vital role in transforming mobility and making our roadways safer and more efficient. Indeed, we ensure String Stability (SS) [5], [6], i.e., the capability of vehicle platoons not to amplify disturbances along the string of vehicles, which results in shock-waves and stop-and-go phenomena mitigation. Without loss of generality, the scenario we consider is an infinite highway where we bypass the needs of identifying and/or following a leader vehicle in a platoon. To this purpose, we consider V2I communications to help provide the needed (macroscopic) information, replacing the leader's one with the result of reducing the total exchanged amount of information.

The authors are with the Laboratory of Signal and Systems (L2S), Centre National de la Recherche Scientifique (CNRS), CentraleSupélec, Paris-Saclay University, 3, rue Joliot-Curie, 91192 Gif-sur-Yvette, France. E-mail: lea.njoua@gmail.com, {jean.auriol, alessio.iovine}@centralesupelec.fr

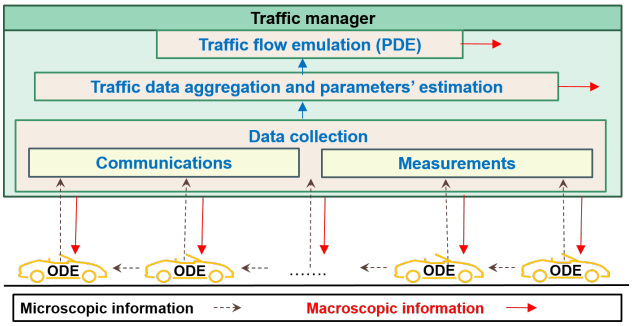

Fig. 1: The considered smart traffic manager and its interaction with the CAVs via V2I communications. It comprises a data collection layer (via communications or measurements), a data aggregation and estimation layer, and a flow emulation layer.

A smart traffic manager is considered to gather and disseminate macroscopic information, both by measuring them or by aggregating transmitted microscopic quantities. It is composed of several layers (see Fig. 1):

- a data collection layer, which gathers the macroscopic information, possibly both using measurements, e.g., via cameras, or V2I communications, e.g., via smartphones or dedicated devices;
- a traffic data aggregation one, which aggregates microscopic quantities into macroscopic ones;
- a traffic flow emulator layer that reproduces the dynamical evolution of the macroscopic traffic flow according to the data collected.

According to the ideas presented in [7], [8] and leveraging the connection among the macroscopic density and the variance of microscopic quantities as relative speed and position as introduced in [9], the smart traffic manager provides the CAVs the macroscopic information that is necessary to ensure string stability. However, because of the utilization of macroscopic information that depends on the whole traffic flow, it is important to remark how the feedback loop implicitly defined by Fig. 1 is similar to when vehicles travel on a ring road [10]–[12]. More precisely, vehicles engage in reciprocal interactions, with the initial vehicle having to take into account the final one for control purposes, similarly as in ring topologies. Although the road's actual geometry may not be circular, CAVs' control structure elicits a similar pattern in vehicle responses, which we term virtual rings [12]. For this reason, in the present paper, we investigate analytical results for string stability in a ring

road without loss of generality compared to the case of an infinite straight highway.

To implement the smart traffic manager, we consider the traffic system from macroscopic and microscopic points of view. The macroscopic model we consider is the second order Aw-Rascle-Zhang (ARZ) one [13]. It uses aggregated state values to express the traffic flow as a fluid using hyperbolic Partial Differential Equations (PDEs). In the meantime, the physical interactions among the vehicles of a platoon are described by Ordinary Differential Equations (ODEs) as a chain of double integrators [5], which express inter-vehicular dynamics. According to the results in [7], [8], the macroscopic information plays the same role in the sharing of the platoon's leader vehicle information (acceleration, speed, or desired speed) for each vehicle. Therefore, an essential reduction in the amount of exchanged information is performed as the vehicles communicate with the infrastructure their microscopic data, and the infrastructure provides the vehicles with aggregate information on the macroscopic variables. For each CAV, the resulting control input is then designed using microscopic quantities that the CAV can measure and a macroscopic quantity that it receives. Therefore, the control action is said to be mesoscopic. The proposed control scheme is based on two levels:

-) at the lower level, each vehicle implements a mesoscopic controller based on the desired distance from the preceding vehicle and a measure of the macroscopic density. Distance and relative speed with respect to the preceding vehicle are supposed to be measured, e.g., by radar or LIDAR, while V2I communications receive the macroscopic information.
-) at the higher level, a centralized traffic manager quantifies macroscopic information and provides it to the vehicles on the highway. The macroscopic information can be measured from the traffic flow, e.g., by using cameras or computed by the received microscopic information from the whole set of vehicles sharing it. In this last case, a data aggregation methodology is needed. Furthermore, the traffic manager simulates the traffic at the macroscopic level via the ARZ model. Therefore, in a receding-horizon-inspired approach, based on the past information (measured or received), it can predict the current state of the traffic and transmit it to the vehicles even in case of missing updates.

To fulfill the goal of a smart manager that empowers mesoscopic controllers for CAVs, the following intermediate steps are provided in the present paper:

1) the extension of ARZ-based simulators to be multi-regime, i.e., to consider both congested and free situations;
2) the definition of a relationship between the categorical traffic models via a bottom-up equivalence. The ODEs describing the microscopic model and the PDEs describing the macroscopic one must match the same reality. Then we
   2a) apply existing algorithms for the aggregation of the microscopic information at the macroscopic level to the ARZ model (see [14]);
   2b) develop a machine learning predictor for estimating fundamental diagram parameters;
3) develop an extension of the analytical investigation of SS proposed in [8] to the case of ring roads. The investigation of ring roads is of interest in the literature since a platoon of vehicles that exhibits unstable dynamics on the ring is string unstable on a straight road [11], [15];
4) introduce a receding-horizon-inspired sharing of the macroscopic information when their measure or the collection of microscopic ones is not available.

Much like the pieces of a mosaic, each aforementioned step presented here is an essential part of the proposed methodology, coming together harmoniously to achieve the primary goal. As far as we are aware, there has been no previous research addressing the specific linkage of establishing a connection between the two models, characterized by multiple ODEs and a PDE, for the purpose of string stability analysis. The traffic manager proposed in this paper bridges the gap between the two levels of information, enabling consideration of the dynamic evolution of the macroscopic model while reducing communication overhead by leveraging V2I communications and a centralized infrastructure tasked with collecting, aggregating, and predicting microscopic data for dissemination to all vehicles. This extends the validation of theoretical findings in [7], [8], where the macroscopic information remains static and fails to address optimal traffic flow objectives.

Compared to recent literature investigating machine learning solutions for PDE problems [16], the present paper only exploits machine learning techniques for the estimation of the parameters of the PDEs while still considering the dynamical evolution to be model-based. Other approaches use physics-informed neural networks but with different classes of macroscopic models, e.g., [17]–[19]. Differently from classical approaches as in [20]–[22], which investigates the existence of analytical solutions for the mixed ODE-PDE problem, we focus on the introduction of macroscopic information in a microscopic framework, thus leading to a mesoscopic dynamical model based on a bottom-up approach, similarly to [8]. Mesoscopic models are a familiar presence in existing literature. Typically, they emerge from integrating microscopic data into macroscopic traffic flow models, following a top-down methodology that targets traffic flow analysis [9]. A common goal is to investigate the impact of microscopic controllers on the traffic flow [23]. Differently, here, the macroscopic information is estimated and adapted to actively provide missing information to ensure SS, which is usually provided by the knowledge of some variables of the leader vehicle, e.g., its desired speed or acceleration. This bottom-up approach is not new in the traffic control literature; however, usually, SS is not investigated, e.g., [24], [25], or is based on a model linearization (see [26], [27]). We leverage previous results on mesoscopic controllers showing the feasibility of the proposed approach [7], [8], and on the possibility of controlling and estimating parameters of a macroscopic ARZ model [28], [29]. The present paper presents similarities with

the work in [30]; however, we explicitly target SS and the identification of miss-matches among the PDEs and the ODEs modeling the traffic, which are not considered in [30].

The rest of the paper is organized as follows. Section II describes the considered macroscopic and microscopic physics-based models and the solution proposed in the current paper for mitigating stop-and-go situations on highways. Section III focuses on the machine learning-based mapping between the microscopic car-following model and the macroscopic ARZ one, describing both the considered approach for aggregating the microscopic information at the macroscopic level and the suggested algorithm for estimating the parameters of the macroscopic model. Section IV introduces rigorous conditions for ensuring string stability in a ring road, which is taken as an approximation of the infinite highway. Also, it provides information on how to use macroscopic quantities obtained from the infrastructure. Section V describes simulations in Python that verify the proposed approach, while Section VI outlines conclusions and perspectives for future works.

II. Modeling

A. Macroscopic traffic model

In transportation systems, macroscopic models have been widely used for simulation, observation, and/or traffic control purpose(s) [31], [9], [13], [14]. They represent the traffic dynamics at an aggregate level using hyperbolic PDEs that govern traffic density and velocity dynamics evolution. The most widely-used macroscopic traffic PDE models include the classical first-order Lighthill-Whitham-Richards (LWR) model [32], [33] and the state-of-art second-order Aw-Rascle-Zhang (ARZ) model [34], [35]. The LWR model corresponds to the conservation law of traffic density. It predicts the formation and propagation of traffic shockwaves on the freeway. Still, it fails to describe the stop-and-go oscillatory phenomenon [36], which causes unsafe driving conditions, increased fuel consumption, and delays in travel time. Subsequently, the second-order ARZ traffic model was conceived to address this stop-and-go traffic pattern, introducing a velocity PDE to augment the LWR model. The ARZ traffic model is characterized by non-linear, second-order hyperbolic PDEs. This category of models underwent extension in works such as [37] and [38], which endeavored to describe freeway traffic within intricate road network configurations.

In the sequel, we embrace the second-order macroscopic ARZ model. We consider a road segment of length $L > 0$. The dynamical evolution of **traffic density** and **velocity** is described as

$$\begin{cases} \partial_t \rho + \partial_x(\rho \upsilon) = 0 \\ \partial_t(\rho(\upsilon + p(\rho))) + \partial_x(\rho\upsilon(\upsilon + p(\rho))) = -\frac{\rho(\upsilon - V(\rho))}{\tau} \end{cases} \tag{1}$$

where $\rho \doteq \rho(x,t)$ is the density and $\upsilon \doteq \upsilon(x,t)$ the velocity over space x and time t, $x \in [0, L]$, $t \in [0, T]$. The **traffic pressure** $p(\rho)$ is defined as an increasing function of the density $p(\rho) = \upsilon_{max}\rho^\eta/\rho_{max}^\eta$. The coefficient η represents the overall drivers' property, reflecting their driving behavior change to the density increase. The positive constant υ_{max} represents the maximum velocity, while the positive constant ρ_{max} is the maximum density defined as the maximum number of vehicles per unit length. The equilibrium density-velocity relation $V(\rho)$ is given by Greenshield's relation [13]:

$$V(\rho) = \upsilon_{max} - p(\rho) = \upsilon_{max}\left(1 - \frac{\rho^\eta}{\rho_{max}^\eta}\right). \tag{2}$$

This relation corresponds to the natural steady-state value of the velocity for a given steady-state density, i.e., for a given steady-state density ρ_{ref}, the corresponding steady-state velocity is given by $\upsilon_{ref} = V(\rho_{ref})$. The positive constant τ is the relaxation time representing the time scale for traffic velocity υ adapting to the equilibrium density velocity relation $V(\rho)$. To regulate freeway traffic and avoid the **stop-and-go oscillatory phenomenon**, different traffic control strategies have been developed and successfully implemented in the literature for the traffic management infrastructures [14], [9]. A complete survey on freeway traffic control can be found in [39]. Boundary controllers using ramp metering have been developed for traffic control of a single freeway segment in [40], [41], [13], [42], [43]. Extensions to road junctions have been proposed in [28], [29], [44].

To simulate the ARZ model (1), we use a two-step Lax-Wendroff algorithm [45], similar to what has been proposed in [13]. As an example, we provide the simulation results of both congested and free traffic conditions below. We consider a simulation time of $T = 60\,\mathrm{s}$, with a sampling of $dt = 0.25\,\mathrm{s}$, and a single-lane road of length $L = 500\,\mathrm{m}$, which is discretized with a space step $dx = 10\,\mathrm{m}$. The reference velocity is $\upsilon_{ref} = 10\,\mathrm{m/s}$ [$36\,\mathrm{km/h}$], while the reference density is $\rho_{ref} = 0.12\,\mathrm{vehicles/m}$ [$120\,\mathrm{vehicles/km}$]. We consider Greenshield's model for speed-density relationships, with $\tau = 60\,\mathrm{s}$ and $\eta = 1$, $\upsilon_{max} = 40\,\mathrm{m/s}$ [$144\,\mathrm{km/h}$] and $\rho_{max} = 0.16\,\mathrm{vehicles/m}$ [$160\,\mathrm{vehicles/km}$].

In the first simulation case (congested regime), we choose the same initial condition as in [13, Chapter 1], i.e., a small amplitude sinusoidal wave acting like a perturbation around the desired density ρ_{ref}. The ongoing and outgoing flow at the boundary of the considered section road, $x = 0$ and $x = L$, are chosen to congest the traffic. Fig. 2 shows the evolution of density and velocity along the road. The fluctuation of density and velocity causes stop-and-go phenomena that can easily be identified. On the contrary, Fig. 3 shows a simulation with similar initial conditions but no inlet flow. We can observe the progressive attenuation of the initial density wave, which tends to stabilize around $0.8\,\mathrm{vehicles/m}$ while the velocity stabilizes around $36\,\mathrm{m/s}$.

B. Microscopic traffic model

Microscopic traffic models, extensively explored in the literature (see [46], [47]), are equally crucial as their macroscopic counterparts. These models delve into individual vehicle dynamics for traffic management, targeting the mitigation of stop-and-go oscillations and shock waves resulting from vehicle behavior [48] and their influence on overall traffic patterns [49], [50], [51]. They are particularly adept at capturing the behavior of vehicle platoons. For the sake

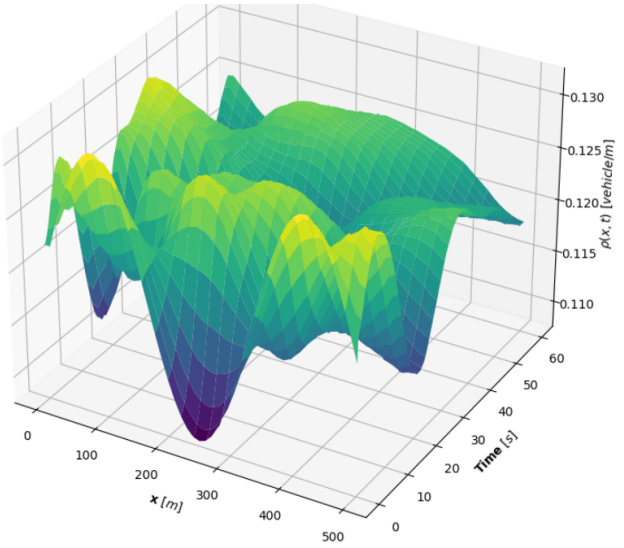

(a) density evolution

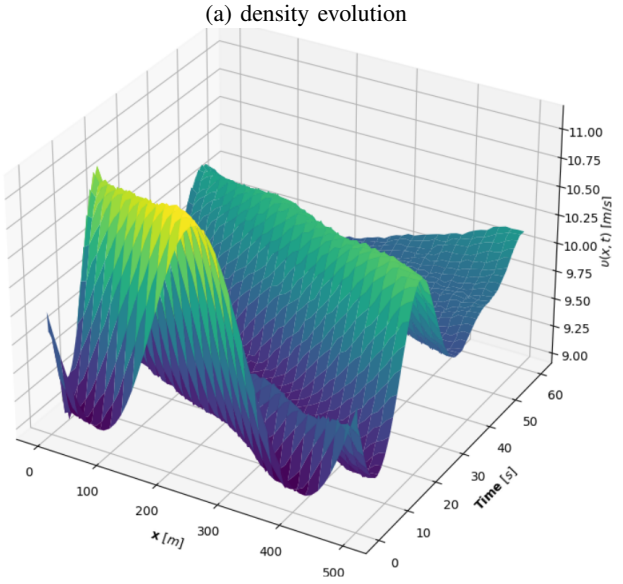

(b) speed evolution

Fig. 2: Density and velocity evolution of the ARZ PDE model in congested regime.

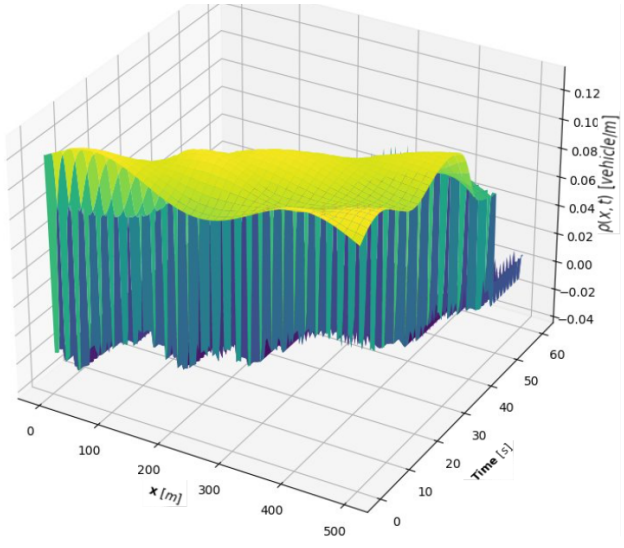

(a) density evolution

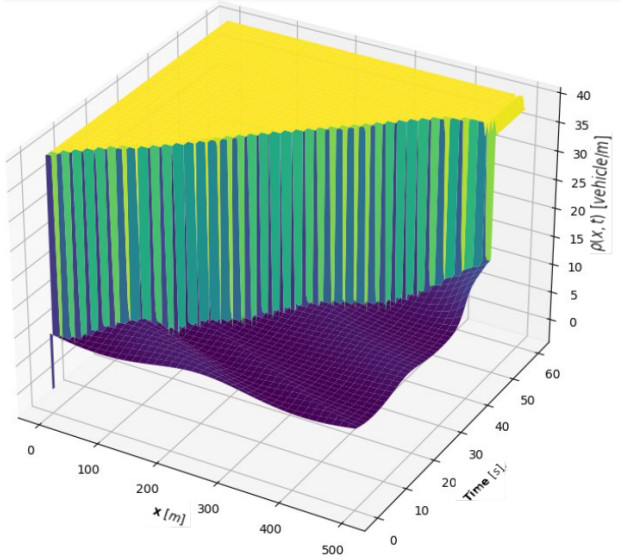

(b) speed evolution

Fig. 3: Density and velocity evolution of the ARZ PDE model in free regime.

of notations, we consider a platoon of vehicles composed of a leader vehicle, denoted with $i = 0$, and a set of follower vehicles, denoted by $\mathcal{I}_N = \{1, 2, ..., N\}$, $N \in \mathbb{N}$, $N > 1$. The resulting set of all the vehicles forming the platoon is defined as $\mathcal{I}_N^0 = \mathcal{I}_N \cup \{0\}$. Each vehicle is characterized by its longitudinal position on the road, $p_i \in \mathbb{R}^+$, and its longitudinal speed, $0 \leq v_i \leq v_{\max}$, $v_{\max} \in \mathbb{R}^+$, $\forall i \in \mathcal{I}_N^0$. Then, we define the state of the $i-$th vehicle as

$$X_i = [\, p_i \;\; v_i \,]^T. \tag{3}$$

The dynamical system corresponding to this scenario neglects both reaction and communication time delays [50], [52], [53], [11]. To offer a comprehensive depiction of the platoon, we employ the predecessor-follower model and account for inter-vehicular interaction by examining the state of each car-following situation between the leading vehicle $i-1$ and the following one i as

$$\chi_i = X_i - X_{i-1} = \begin{bmatrix} \Delta p_i \\ \Delta v_i \end{bmatrix} = \begin{bmatrix} p_i - p_{i-1} \\ v_i - v_{i-1} \end{bmatrix}, \quad i \in \mathcal{I}_N^0. \tag{4}$$

The resulting microscopic dynamical model of the $i-$th car-following, i.e., predecessor-follower, pair is [52]

$$\dot{\chi}_i = \begin{bmatrix} \Delta \dot{p}_i \\ \Delta \dot{v}_i \end{bmatrix} = \begin{bmatrix} \Delta v_i \\ u_i - u_{i-1} \end{bmatrix}, \; i \in \mathcal{I}_N^0, \tag{5}$$

where u_i is the input representing both the acceleration and brake actions of vehicle i, and u_{i-1} is considered received via V2V communications or estimated by vehicle i, e.g., using LIDAR technology. To define the equilibrium point of the platoon, we consider the constant speed hypothesis for the virtual leader $i = -1$ (see [54] and [55]). Let us denote $\bar{v} > 0$ as a constant speed. Then $p_{-1}(t) = \bar{v} \cdot t$, $v_{-1}(t) =$

$\bar{v},\ u_{-1}(t) = 0,\ \forall t \geq 0$. Assuming that $\Delta\bar{p} > 0$ is the desired inter-vehicular distance at the steady-state condition and that $\Delta p_0(t) = -\Delta\bar{p} \quad \forall\, t \geq 0$, then the equilibrium point for the $i-$th system of dynamics (5) corresponds to the case where all the vehicles have the same speed and are at the same distance,

$$\chi_{e,i} = [-\Delta\bar{p}\ 0]^T,\ \forall\, i \in \mathcal{I}_N^0. \tag{6}$$

Since the state vector (4) is defined with respect to the follower vehicle, then the distance Δp_i and the relative speed Δv_i have opposite signs. For this reason, the equilibrium distance in (6) is $-\Delta\bar{p} < 0$. From the platoon point of view, we define the lumped state and the lumped equilibrium point for $u_{-1} = 0$ respectively as

$$\chi = [\chi_0^T\ \chi_1^T \cdots \chi_N^T]^T \tag{7}$$

and

$$\chi_e = [\chi_{e,0}^T\ \chi_{e,1}^T\ \cdots\ \chi_{e,N}^T]^T = [\bar{\chi}^T\ \bar{\chi}^T \cdots \bar{\chi}^T]^T. \tag{8}$$

C. String Stability and other definitions

Several concepts are needed to describe the control goals for microscopic models. We refer to [6] for an overview of the subject, where several definitions of String Stability (SS) and Asymptotic String Stability (ASS) can be found. Another definition of interest in this paper is the Disturbance String Stability (DSS) [5]. In the sequel, we denote P_{cl} the closed-loop system.

Definition 1: (String Stability) The equilibrium $\chi_{e,i}, i \in \mathcal{I}_N^0$, of P_{cl} is said to be String Stable if, for any $\epsilon > 0$, there exists $\delta > 0$ such that, for all $N \in \mathbb{N}$, for all $t \geq 0$,

$$\max_{i\in\mathcal{I}_N^0} |\chi_i(0) - \chi_{e,i}| < \delta \Rightarrow \max_{i\in\mathcal{I}_N^0} |\chi_i(t) - \chi_{e,i}| < \epsilon. \tag{9}$$

Definition 2: (Asymptotic String Stability) The equilibrium $\chi_{e,i},\ i \in \mathcal{I}_N^0$, of P_{cl} is said to be Asymptotically String Stable (ASS) if it is String Stable and, for all $N \in \mathbb{N}$,

$$\lim_{t\to\infty} |\chi_i(t) - \chi_{e,i}| = 0, \quad \forall\ i \in \mathcal{I}_N^0. \tag{10}$$

Definition 3: (Disturbance String Stability) The equilibrium $\chi_{e,i},\ i \in \mathcal{I}_N^0$, of P_{cl} is said to be Disturbance String Stable (DSS) if there exist functions β_d of class $\mathcal{KL}$ and σ_d of class $\mathcal{K}_\infty$ and constants $\delta > 0$, $\delta_d > 0$, such that, for any initial condition $\chi_i(0)$ and disturbance $\bar{d}_i$ satisfying

$$\max_{i\in\mathcal{I}_N^0} |\chi_i(0) - \chi_{e,i}| < \delta,\ \max_{i\in\mathcal{I}_N^0} |\bar{d}_i(\cdot)|_\infty^{[0,t]} < \delta_d \tag{11}$$

the solution $\chi_i(t)$ exists for all $t \geq 0$ and satisfies

$$\begin{aligned}\max_{i\in\mathcal{I}_N^0} |\chi_i(t) - \chi_{e,i}| \leq\ & \beta_d\left(\max_{i\in\mathcal{I}_N^0} |\chi_i(0) - \chi_{e,i}|, t\right) \\ & + \sigma_d\left(\max_{i\in\mathcal{I}_N^0} |\bar{d}_i(\cdot)|_\infty^{[0,t]}\right)\ \forall\, N \in \mathbb{N}.\end{aligned} \tag{12}$$

In the sequel, we aim to show DSS for the ring road configuration where the disturbances model errors in the transmission of the data or the consideration of an averaged value for the macroscopic function compared to a function tailored for each vehicle i. To shed light on the distribution of control effort between microscopic and macroscopic variables, we specifically examine the scenario without disturbances, where tailored macroscopic information is available for each CAV. In this context, we outline conditions for ASS, which elucidate the balance required between the weighting of microscopic and macroscopic information for control applications.

D. Proposed solution: the smart traffic manager

To mitigate stop-and-go oscillations and prevent freeway congestion caused by phenomena like shock waves, the proposed approach emphasizes minimal information sharing by enabling CAVs to receive macroscopic information. Therefore, we are able to implement mesoscopic controllers and ensure DSS, facilitated by the multi-level control scheme that is enabled considering the suggested smart traffic manager.

At the higher level, the smart traffic manager collects and transmits real-time macroscopic data via V2I communication or measurements. In instances of missing data or transmission issues, a receding-horizon-like approach generates macroscopic predictions based on past measurements, communicated data, and the system's dynamic evolution using the ARZ model. At the lower level, CAVs utilize macroscopic information to compensate for the absence of a platoon leader sharing key knowledge for DSS. Leveraging previous SS results, we ensure ring string stability through mesoscopic controllers.

Mesoscopic controllers are at the interface between macroscopic and microscopic models and offer significant advantages in vehicular platoon control. However, employing such controllers requires effectively expressing physical macroscopic information to define control inputs [7]. Both microscopic and macroscopic models depend on specific constant parameters. Their initial conditions and state variables differ from one another, considering the same traffic conditions. Our goal is to establish a coherent link between microscopic predecessor-following (i.e., car-following) models, encompassing initial conditions, model parameters, and state variables of freeway traffic, and the macroscopic ARZ model, ensuring consistency across traffic conditions. This linkage ensures a consistent logical and numerical portrayal of the identical physical process across time. We can confidently incorporate accurate macroscopic information into the microscopic controller by achieving this coherence. This integration allows us to retrospectively assess enhancements in the microscopic evolution, presenting a novel and significant challenge in the mixed ARZ and car-following model research arena.

III. Estimation

A. Aggregation of microscopic information

The objective of this section is to reconstruct macroscopic variables from microscopic ones via the process of aggregation. More precisely, using the data of a microscopic model, we want to obtain the macroscopic variables corresponding to the ARZ model. Several approaches have already been proposed in the literature (see [9, chapter 6], [14], [56]). More specifically, among other techniques, we targeted:

- The gradient expansion or Taylor approximations approach. It is useful for linear analysis, but its validity

is limited by the fact that it requires small gradients, and this does not fit the traffic jam situation, especially the presence of negative speed.
- The linear interpolation approach. It performs well in practical simulations but suffers from inconsistency since the conservation of the vehicle's number property is not respected, and the corresponding macroscopic model is too isotropic.
- A smooth particle hydrodynamics reminding approach; it is a well-consistent approach that provides non-local macroscopic derivation models. However, it usually suffers from high complexity and requires significant computation time.

1) Smooth Particle Hydrodynamics: The approach we consider in this paper is adjusted from the smooth particle hydrodynamics approach sketched in [14]. We describe here the relationships between the state variables of each autonomous vehicle as described in (3) and the macroscopic ones used in the definition of the ARZ model (1). We follow the algorithm described in [14]. Let us consider a longitudinal discrete space x at time t. We denote by i and $i-1$ the nearest surrounding vehicles in the platoon at that time t. Respectively denoting p_i and v_i the position and speed of vehicle i at time t, we have that $p_i \leq x < p_{i-1}$, (p_i, v_i) . Then, the macroscopic average velocity $v(x,t)$ is defined as

$$v(x,t) = \frac{v_i(t)[p_{i-1}(t) - x] + v_{i-1}(t)[x - p_i(t)]}{p_{i-1}(t) - p_i(t)}, \quad (13)$$

while its partial derivative with respect to x reads

$$\frac{\partial v}{\partial x} = \frac{v_{i-1}(t) - v_i(t)}{p_{i-1}(t) - p_i(t)}. \quad (14)$$

The density $\rho(x,t)$ is finally defined as

$$\frac{1}{\rho(x,t)} = \Delta p_{min} + \frac{s_i(t)[p_{i-1}(t) - x] + s_{i-1}(t)[x - p_i(t)]}{p_{i-1}(t) - p_i(t)} \quad (15)$$

where $s_i(t) = s\left(p_i(t), x(t)\right)$ is the smoothing function around a point $x(t)$, and Δp_{min} is the minimum distance between two consecutive vehicles. This aggregation model will be used to define the initial conditions of the ARZ model. Below, we present a numerical example to illustrate the proposed approach. Consider a platoon of vehicles actuated using classical PID controllers (not necessarily ensuring ASS). We aggregated the initial microscopic data before running the ARZ simulator. Figure 4 shows the resulting values of density and average speed. We notice the initial irregularity in the simulation when the platoon is introduced. Over time, the curves representing density and velocity gradually smooth out and remain consistent, indicating the stability of the platoon. In this simulation example, the different constant parameters required in the ARZ model have been tuned following the procedure presented in the next subsection.

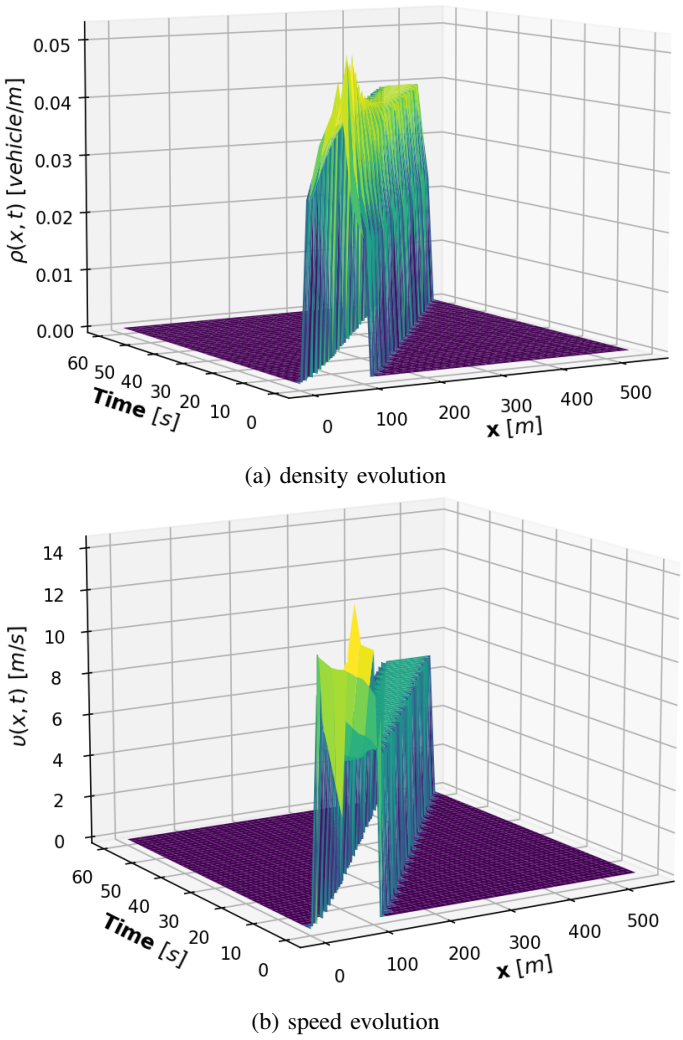

(a) density evolution

(b) speed evolution

Fig. 4: The evolution of the density (a) and the speed (b) over time of an isolated platoon in a section of road.

B. ARZ parameters' estimation

Due to the necessity of adapting the ARZ model to fit possibly changing traffic or street conditions, we need to estimate some key parameters of the model easily. Specifically, we target to estimate the function $V(\rho)$ in equation (1), representing the density-speed equilibrium relationship. To this purpose, we consider the analytical expression of $V(\rho)$ given by the Greenshield's model (2) with $\eta = 1$ (to simplify the analysis). The maximum speed, v_{max}, and the maximum density, ρ_{max}, are the targeted parameters we want to estimate. Several classical calibration methods are available in the literature, e.g., least square (LS), weighted least square (WLS) or Linear Regression (LR). However, they focus on a single traffic regime, are sensitive to noise, and are often computationally time-demanding. On the contrary, we aim to develop a calibration method that is less sensitive to noise and that could be run in real-time without being over-sensitive to variations in the traffic conditions for platoons, thus being multi-regime. As this is our objective, we contrast the potential outcomes and performance of state-of-the-art algorithm LR with those generated by a machine learning approach based on Deep Neural Networks (DNN). This comparison allows us to identify the strengths and weaknesses of each approach before determining the preferred option. Therefore, we investigate a

machine learning approach for estimating ARZ parameters, namely maximum density and maximum speed using the highest frequencies of the signals describing the most important characteristics of traffic behavior. We consider the 1D high-frequency estimation method developed in [57], [58] for a PDE estimation task, which considers the Fourier transform (see [59], [60]), and extend it for 2D datasets.

Aggregated or not, whether simulated, collected from sensors, or provided directly by the CAVs, the considered output data (macroscopic density $\rho(x,t)$ and velocity $\upsilon(x,t)$) are spatio-temporal and somehow depend on Greenshield's function parameters υ_{max} and ρ_{max} that we want to estimate. According to the considered road length simulation time or historical data, this available 2D dataset could not be easy to use for the required active memory space and processing time. However, the spectrum of the macroscopic density $\rho(x,t)$ and velocity $\upsilon(x,t)$ should contain sufficient information to distinguish the two relevant parameters υ_{max} and ρ_{max}. By applying a Fast Fourier Transform (FFT) to the functions $\rho(x,t)$ and $\upsilon(x,t)$, we can obtain their spectra. The 2-dimensional Fast Fourier Transform (FFT2) $F(w,z)$ of an input signal $f(x,t)$ is defined in the frequency coordinate (w,z) by

$$F(w,z) = \iint f(x,t) * e^{-i2\pi(wx+zt)} dxdt. \tag{16}$$

The function F is a complex function that corresponds to the spectrum of the signal f. Several attributes characterize it. Among them, we can cite the dominant peak, the number of peaks, and the corresponding frequencies. The values of some of these attributes are related to the parameters υ_{max} and ρ_{max} we want to estimate. Thus, for a set of known parameters that characterize the driver's behavior (reference speed, reference density, input traffic flux, output traffic flux), we can run thousands of simulations, modifying the parameters between each simulation. This gives us a set of data (known as the training set) for which the correct values of the parameters υ_{max} and ρ_{max} are known. The suggested algorithm will learn from this data set and find suitable correlations between the previously defined attributes and the unknown parameters. Once adequately trained, the algorithm can be applied to make accurate predictions for new data sets. Before training the machine learning estimation algorithm, we need to design an algorithm that can extract the relevant attributes from the available $2D$ datasets. The proposed algorithm is described in Algorithm 1, where we denote the input signal by $f(x,t)$, where (x,t) represents the spatio-temporal coordinates. As first step, we compute the 2-dimensional Fast Fourier Transform (FFT2) Then, we move the zero frequency to the center of the $F(w,z)$ by computing

$$F_{shifted}(w,z) = F(w,z) * e^{\pi(w+z)}. \tag{17}$$

As a third step, according to what is described in [60, chap. 4], we calculate the magnitude of the shifted Fourier Transform $F_{shifted}$ to obtain the magnitude spectrum $|F_{shifted}(w,z)|$. Then, we flatten the magnitude spectrum and sort it in descending order. Here, we denote by s the flattened and sorted array of magnitude spectrum values. By selecting the n highest frequency, we determine the threshold value and set a threshold value $\bar{s}$ such that $\bar{s}$ is the n-th highest value in s, that is $\bar{s} \leftarrow s[n]$. We can then append to our list values of magnitude (and their coordinates (w,z)) that are greater or equal to $\bar{s}$. We define by highFreqList that list. This list will contain the relevant attributes to train the learning algorithms.

Algorithm 1 2D-Signal-High-Frequencies-Extraction

procedure 2D-SIHIFREX($f(x,t), n$)
  $F(w,z) \leftarrow \iint f(x,t) * e^{-i2\pi(wx+zt)} dxdt$
  $F_{shifted}(w,z) \leftarrow F(w,z) * e^{\pi(w+z)}$
  $s \leftarrow descendingSort(magnitudeSpectrumF(w,z))$
  $\bar{s} \leftarrow s\,[n]$
  $highFreqList = []$
  for w, z in dim($F_{shifted}$) **do**
    $freq_{wv} \leftarrow F_{shifted}(w,z)$
    if $freq_{wz} \geq \bar{s}$ **then**
      $highFreqList.append([freq_{wz}, w, z])$
    end if
  end for
  return highFreqList
end procedure

1) Dataset: origin and characteristics: We generate training data by simulating the PDE ARZ model using different initial conditions, different pairs of values (maximum speed, maximum density), but also different reference speeds and densities, input traffic flux, and output traffic flux. For each simulation, we extract the $n = 10$ highest frequencies using algorithm 1.

2) Models and training: We aim to predict the maximum speed and maximum density from traffic data. Because of the considerable volume of data and its complexity, we opted for comparing two methods, namely (LR) and (DNN), and describe advantages and drawbacks before pointing out the preferred choice. Indeed, the variation of initial conditions and boundary conditions on a considered section road produces a quite different profile of density and velocity for the fixed couple $(\rho_{max}, \upsilon_{max})$. For the LR, we used a TensorFlow Keras normalization layer and one dense layer of 2 neurons for output prediction (since we have two parameters to estimate). On the other hand, the neural network model is built with a normalized layer, 6 hidden layers, and an output layer with two neurons. We used the function *tanh* as the activation function for all units in the hidden layer. After careful evaluation of several options, the hidden layers have been chosen to have 100 neurons, 90 neurons, and 64 neurons for the remaining four layers. For both models, 1200 entries of the dataset have been shuffled and split into 80% for training and 20% for testing. The training set is internally divided into the actual training set and validation set. Trained for 400 epochs for the linear model and 1000 epochs for the DNN. Noise was added to the different data.

3) Results and validation: The training and validation losses are shown in Fig.5 and Fig.6 for linear regression and the DNN, respectively. We recall here that the training loss is the error computed by the DNN to compare the training set examples with the model, taking into account

the estimated parameters at that epoch of training. While the validation loss is the error obtained predicting the validation set using the model at the related epoch. Both trained models exhibit certain similarities but also manifest differences. At first, their validation losses and losses during training decrease exponentially, maintaining a consistent rate and convergence. This indicates an absence of risks related to underfitting or overfitting. Nevertheless, the differences are worth noting.

As depicted in Fig. 5(a), although the LR model's losses (validation, test) decrease exponentially from 18 to 0.7 within 10 epochs, they plateau between 0.23 and 0.66 until the final epoch. On the other hand, the losses of the DNN decrease exponentially from 17 to a value below 2 around the 25th epoch (see Fig. 6(a)). Subsequently, it follows a non-linear yet nearly exponential decline to an error of 0.055 at 100 epochs, with further gradual convergence to 0.04.

Another point to be mentioned is the comparison between the test results for predicting maximum density (ρ_{max}) and maximum speed (v_{max}). This is illustrated in Fig. 5(b) and 6(b), which show predictions versus true values plots. Here, the closer the elements are to the diagonal, the better the prediction. In the considered case, Fig. 5(b) well exhibits the weakness of the linear regression on generalizing the density, although the performance on maximal velocity is acceptable. On the contrary, Fig. 6(b) shows how the DNN clearly outperforms the linear regression in predicting maximal density and maximal velocity at the same time. This starkly highlights the superior performance of the DNN over the LR model and, therefore, leads to DNN selection.

For the sake of completeness, we provide here a few details on the training time. The CPU time is 37.4 s for LR and 136 s for DNN. The total time needed has been of 41.7 ss for LR and 203 s for DNN. The mean absolute error is 0.632274 for the LR and 0.037741 for the DNN. The test set accuracy is convincing, highlighting the DNN model's superior predictive performance compared to the linear one. Exploring the optimal high-frequency number represents a potential avenue for future investigation.

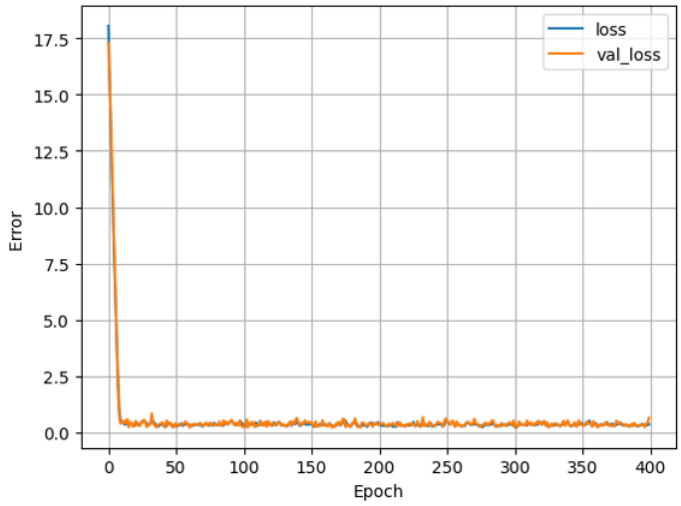

(a) Training and validation losses: $loss$ and val_{loss}, respectively.

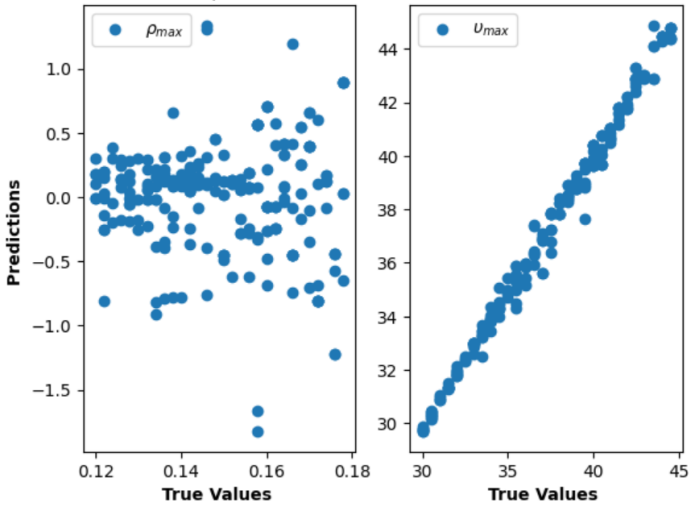

(b) Test set prediction VS true values.

Fig. 5: FFT2 dataset: Loss and validation loss (a) during training, and test set prediction (b) on trained LR.

IV. String stability for ring road

A. Ring road and macroscopic information modeling

When implementing a feedback controller that considers an averaged value of the macroscopic density, vehicles engage in reciprocal interactions where the leading vehicles are influenced by the trailing ones. Consequently, even if the road geometry is not circular, the control structure of CAVs generates a pattern resembling ring topologies in vehicle responses. For this reason, it is of interest to investigate DSS for ring roads, also named ring stability. Differently from the case of a platoon on a straight road with a leader vehicle, the ring road configuration cuts the possibility to start investigating stability from the head of the platoon and forces to consider the whole set of vehicles as equal. To maintain consistency with the modeling in Section II-B, we adopt a slight abuse of notation by considering the predecessor of vehicle 0 to be vehicle N. In other words, for $i = 0$, we treat $i - 1$ as N.

Let us define the function ψ as describing at the microscopic level the error between the average macroscopic information related to the density and average velocity in a portion of the road compared to the ideal one. To simplify the notation, we focus on the density dependence $\psi(\rho)$ as we consider the average velocities to have a less significant contribution to velocity. Clearly, from the perspective of the CAV i, this averaged quantity can be seen as the sum of a tailored function $\psi_i(\rho)$, which is computed specifically for the leader vehicles of the CAV i considering the ideal neighborhood providing the most effective information for ensuring SS, plus a disturbance d_i:

$$\psi(\rho) = \psi_i(\rho) + d_i. \tag{18}$$

To highlight the dual nature of the variable ψ, we remark that it is expressed as $\psi = \psi(\rho)$ from a macroscopic point of view while as $\psi = g(\chi)$ from a microscopic perspective (where χ is defined in equation (7)), thus leveraging the dependence on an averaged value concerning the entire platoon. Therefore, it is possible to express the relationship $\psi(\rho) = g(\chi)$. In contrast, for a tailored function, it depends

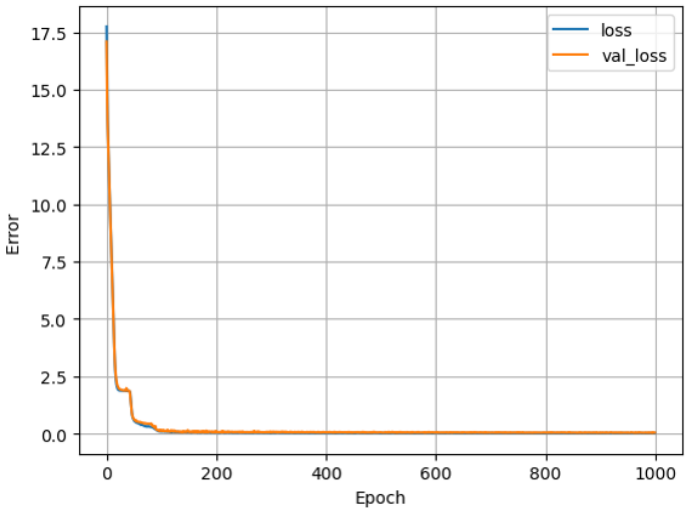

(a) Training and validation losses: $loss$ and val_{loss}, respectively

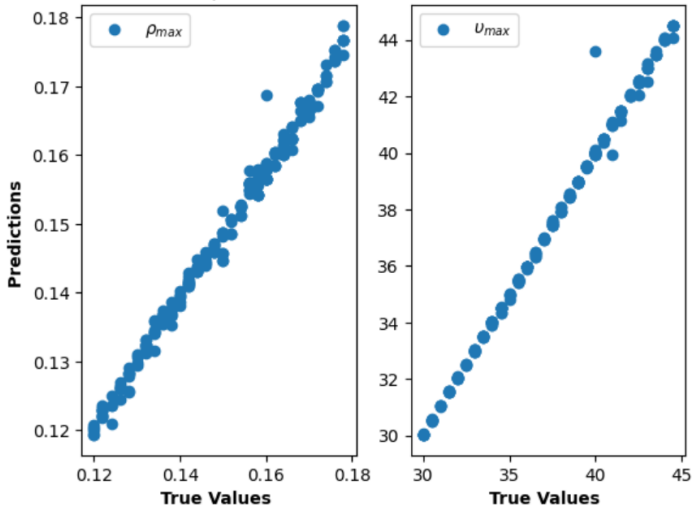

(b) Test set prediction VS true values.

Fig. 6: FFT2 dataset: Loss and validation loss (a) during training, and test set prediction (b) on trained DNN.

solely on the vehicles within the relevant neighborhood, e.g., $\psi_i(\rho) = g(\chi_0, ..., \chi_{i-1})$ in a string configuration as in [7].

Remark 1: Similarly to [7], [8], it is worth noticing that the average and variance of microscopic parameters are related to macroscopic traffic variables, such as traffic density, which is defined as the reciprocal of the mean inter-vehicle distance [61, ch. 2, p. 26]. Furthermore, various diagrams illustrate the relationships between local and global factors, including the speed-density diagram [9, ch. 4]. Therefore, it is realistic to consider a connection among these quantities and that the function $\psi(\rho)$ obeys to condition on the boundedness to the maximum values of the interconnected systems. Then, it is possible to write that $\psi_i(\rho)$ can be modeled as a $\mathcal{K}_\infty$ function, e.g., $\gamma_i \in \mathcal{K}_\infty$, with γ_i such that it results

$$\psi_i(\rho) = \gamma_i \left(\max_{j \in \mathcal{I}_N^0} |\chi_j(\cdot)|_\infty^{[t_0,t]} \right), \tag{19}$$

and that there exists a constant $\gamma \in (0, 1)$ such that

$$\gamma_i(s) \leq \gamma s. \tag{20}$$

The mesoscopic controller we consider for each CAV is in the form of

$$u_i = h_i(\psi(\rho), \chi_i, \chi_{e,i}, u_{i-1}) \tag{21}$$

where χ_i in (4), $\chi_{e,i}$ in (6), u_{i-1} and the $\psi(\rho)$ describing the evolution of the macroscopic density are the inputs of the system, while h_i is the output function used to compute the control input u_i. We suppose the value of $\psi(\rho)$ is communicated to each CAV by the smart traffic manager via V2I communications. Since the function ψ verifies $\psi = g(\chi)$, the interconnected closed loop system for each CAV is in the form of

$$\dot{\chi}_i = f_{cl}(\chi_i) + g_{cl,i}(\chi), \ \ \forall\, i \in \mathcal{I}_N^0, \tag{22}$$

where the generic functions $f_{cl}(\chi_i)$ and $g_{cl,i}(\chi)$ can be easily computed once the formulation of the mesoscopic controller is introduced. The modeling we consider for each CAV in a ring road is consistent with the ones considered in [11], [12]. In the sequel, we show DSS of the model in (22) by taking into account the disturbance d_i in (18).

Remark 2: If we consider the control input u_{i-1} not to be exactly known, it is possible to define it as the sum of a known quantity $\tilde{u}_{i-1}$ and a bounded disturbance $\tilde{d}_i$, i.e.,

$$u_{i-1} = \tilde{u}_{i-1} + \tilde{d}_i. \tag{23}$$

Then, we can refer to the case of known value by defining the disturbance $\hat{d}_i$ as the sum of the uncertainties on the macroscopic variable and on the microscopic control input:

$$\hat{d}_i = d_i + \tilde{d}_i. \tag{24}$$

B. Theoretical result

In this section, according to the model in (18) and (22), we examine an idealized case where each CAV possesses perfect knowledge of the macroscopic function, even though it is affected by a disturbance that deviates it from this ideal model. This disturbance represents a realistic situation where the knowledge of the macroscopic function is not perfectly aligned with each CAV's specific position, but it provides an averaged value over a road segment. We incorporate insights from prior research to establish that the resulting system maintains the DSS property. Furthermore, we extend the analysis to an even more constrained ideal scenario, i.e., one that excludes disturbances. By doing so, we offer guidance on how to allocate control efforts between microscopic and macroscopic information utilization.

For the sake of clarity, we refer to the controller u_i implementing constant spacing policy in [7] but modify the tailored function describing macroscopic information with the averaged one $\psi(\rho)$. However, the result introduced here is general and not limited by this particular choice of controller or spacing policy. Let the control u_i be defined as

$$\begin{aligned} u_i = u_{i-1} + \Delta \dot{v}_i^r - K_{\Delta v}(\Delta v_i - \Delta v_i^r) \\ - (\Delta p_i + \Delta \bar{p}) - \psi(\rho), \end{aligned} \tag{25}$$

where $\Delta\bar{p}$ is the desired equilibrium in $\chi_{e,i}$ in (6), and Δv_i^r is defined as

$$\Delta v_i^r = -K_{\Delta p}(\Delta p_i + \Delta\bar{p}). \tag{26}$$

We consider the constant values $K_{\Delta p} > 0$ and $K_{\Delta v} > 0$ as desired control gains. We name the controller u_i in (25) a mesoscopic controller, since it considers both microscopic quantities as distance and relative speed as well as the macroscopic quantity $\psi(\rho)$.

Remark 3: The functions $f_{cl}(\chi_i)$ and $g_{cl,i}(\chi)$ of the closed loop system in (22) when considering u_i in (25) result:

$$f_{cl}(\chi_i) = \\ = \begin{bmatrix} \Delta v_i \\ -(K_{\Delta v} + K_{\Delta p})\Delta v_i - (1 + K_{\Delta v}K_{\Delta p})(\Delta p_i + \Delta\bar{p}) \end{bmatrix}$$

$$g_{cl,i}(\chi) = \begin{bmatrix} 0 \\ -\psi(\rho) \end{bmatrix}.$$

Theorem 1: Let us consider the system $\chi = [\chi_0^T\, \chi_1^T \dots \chi_N^T]^T$ representing a platoon of vehicles in a ring road, where the dynamical system χ_i in (5), for $i \in \mathcal{I}_N^0 = \{0, 1, 2, ..., N\}$, $N \in \mathbb{N}$, $N > 1$, describes a predecessor-follower interaction between vehicles $i-1$ and i, respectively, along the platoon, i.e.,

$$\dot{\chi}_i = \begin{bmatrix} \Delta v_i \\ u_i - u_{i-1} \end{bmatrix},\ i \in \mathcal{I}_N^0,$$

with $i-1 = N$ for $i = 0$, and with the control input u_i defined as in (25):

$$\begin{aligned} u_i =& u_{i-1} + \Delta\dot{v}_i^r - K_{\Delta v}(\Delta v_i + K_{\Delta p}(\Delta p_i + \Delta\bar{p})) \\ & - (\Delta p_i + \Delta\bar{p}) - \psi(\rho), \end{aligned}$$

where $\Delta\bar{p}$ is the desired spacing policy to track and $\psi(\rho)$ describes the macroscopic information. Let $\psi(\rho)$ be defined as in (18), i.e., as the sum of a tailored information for the vehicle i and a disturbance d_i, $\psi(\rho) = \psi_i(\rho) + d_i$, where $\psi_i(\rho)$ is equivalent to a function aggregating microscopic quantities:

$$\psi_i(\rho) = g(\chi) = \gamma_i\left(\max_{j\in\mathcal{I}_N^0} |\chi_j(\cdot)|_\infty^{[t_0,t]}\right).$$

Let $\psi(\rho)$ be bounded as composed by bounded quantities, and such that there exists a $\gamma \in (0,1)$, with $\gamma_i(s) \le \gamma s$. Then, the resulting closed-loop system is DSS.

Proof 1: Let us describe the closed loop system dynamics of the follower i with the equilibrium point $\chi_{e,i}$ in (6). We investigate stability via the candidate Lyapunov function W_i as

$$W_i = W_{i,1} + W_{i,2} = \frac{(\chi_{i,1} + \Delta\bar{p})^2}{2} + \frac{(\chi_{i,2} - \chi_{i,2}^r)^2}{2}, \tag{27}$$

where, according to (26), the value $\chi_{i,2}^r$ is defined as

$$\chi_{i,2}^r = -K_{\Delta p}(\chi_{i,1} + \Delta\bar{p}). \tag{28}$$

The time derivative $\dot{W}_i$ reads

$$\begin{aligned} \dot{W}_i =& \dot{W}_{i,1} + \dot{W}_{i,2} \\ =& (\chi_{i,1} + \Delta\bar{p})\chi_{i,2} \\ & + (\chi_{i,2} - \chi_{i,2}^r)(\dot{\chi}_{i,2}^r - K_{\Delta v}(\chi_{i,2} - \chi_{i,2}^r)) \\ & + (\chi_{i,2} - \chi_{i,2}^r)(-(\chi_{i,1} + \Delta\bar{p}) - \psi(\rho) - \dot{\chi}_{i,2}^r). \end{aligned} \tag{29}$$

By adding and removing $(\chi_{i,1}+\Delta\bar{p})\chi_{i,2}^r$, and considering (28) and (18), we obtain

$$\begin{aligned} \dot{W}_i =& (\chi_{i,1} + \Delta\bar{p})(\chi_{i,2} + \chi_{i,2}^r - \chi_{i,2}^r) \\ & - K_{\Delta v}(\chi_{i,2} - \chi_{i,2}^r)^2 \\ & + (\chi_{i,2} - \chi_{i,2}^r)(-(\chi_{i,1} + \Delta\bar{p}) - \psi(\rho)) \\ =& - K_{\Delta p}(\chi_{i,1} + \Delta\bar{p})^2 - K_{\Delta v}(\chi_{i,2} - \chi_{i,2}^r)^2 \\ & - (\chi_{i,2} - \chi_{i,2}^r)(\psi_i(\rho) + d_i). \end{aligned} \tag{30}$$

Then, by Young's inequality, we obtain

$$\begin{aligned} \dot{W}_i \le& - K_{\Delta p}(\chi_{i,1} + \Delta\bar{p})^2 - K_{\Delta v}(\chi_{i,2} - \chi_{i,2}^r)^2 \\ & + ||\chi_{i,2} - \chi_{i,2}^r||^2 + \frac{||\psi_i(\rho)||^2}{2} + \frac{||d_i||^2}{2} \\ \le& - K_{\Delta p}||\chi_{i,1} + \Delta\bar{p}||^2 - (K_{\Delta v} - 1)||\chi_{i,2} - \chi_{i,2}^r||^2 \\ & + \frac{||\psi_i(\rho)||^2}{2} + \frac{||d_i||^2}{2}. \end{aligned} \tag{31}$$

Then, from the quadratic structure of the time derivative in (31), there exist functions $\beta_i^W \in \mathcal{KL}$, and $\gamma_i^W, \theta_i^W \in \mathcal{K}_\infty$ such that the following inequality holds

$$\dot{W}_i(\tilde{\chi}_i(t)) \le -\beta_i^W(|\tilde{\chi}_i(t_0)|) + \gamma_i^W(|\psi_i(\rho)|) + \theta_i^W(|d_i|), \tag{32}$$

where $\tilde{\chi}_i = \chi_i - \chi_{e,i}$. Then, from (32) it follows that the Input-to-State Stability (ISS) condition is satisfied [62, Theorem 4.19]. Therefore, by considering (19) it results

$$\begin{aligned} |\tilde{\chi}_i(t)| \le& - \beta_i\left(|\tilde{\chi}_i(t_0)|, t\right) + \gamma_i\left(\max_{j\in\mathcal{I}_N^0} |\tilde{\chi}_j(\cdot)|_\infty^{[t_0,t]}\right) \\ & + \theta_i\left(|d_i(\cdot)|_\infty^{[t_0,t]}\right),\ t \ge t_0 \ge 0, \end{aligned} \tag{33}$$

where $\beta_i \in \mathcal{KL}$, and $\gamma_i, \theta_i \in \mathcal{K}_\infty$, and (19) describing the contribution of $\psi_i(\rho)$. Since (33) holds for all $i \in \mathcal{I}_N^0$ and there exists a $\gamma \in (0,1)$ such that $\gamma_i(s) \le \gamma s$, then it is possible to apply Theorem 1 in [63] to prove that

$$\begin{aligned} \max_{i\in\mathcal{I}_N^0} |\tilde{\chi}_i(t)| \le& \beta_d\left(\max_{i\in\mathcal{I}_N^0} |\tilde{\chi}_i(0)|, t\right) \\ & + \sigma_d\left(\max_{i\in\mathcal{I}_N^0} |d_i(\cdot)|_\infty^{[0,t]}\right)\ \forall\, N \in \mathbb{N}. \end{aligned} \tag{34}$$

for some function $\beta_d \in \mathcal{KL}$ and $\sigma_d \in \mathcal{K}_\infty$. This concludes the proof. ■

Therefore, it is possible to ensure DSS in a ring road configuration via the utilization of averaged macroscopic information, where the disturbance describes the difference with ideal macroscopic information that is tailored for each CAV. In the case $d_i = 0$, these results prove ASS.

C. Practical suggestions on how to weight microscopic and macroscopic information in control strategies

Given the dual significance of both levels of information in achieving shock-wave harmonization, it is essential to determine the appropriate balance in control strategies between them. To shed light on this optimal trade-off on which information to rely more for control purposes, we examine the required conditions under a more constrained scenario. Specifically, we

analyze the case with customized macroscopic information for each CAV, assuming the absence of external disturbances, i.e., $d_i = 0$: $\psi(\rho) = \psi_i(\rho) = g_{cl,i}(\chi)$. Therefore, the mesoscopic controller in (25) can be rewritten as

$$u_i = u_{i-1} + f_u(\tilde{\chi}_i) + g_{cl,i}(\tilde{\chi}) \tag{35}$$

The purpose here is to weight the contribution of the functions f_u and $g_{cl,i}$, representing the control effort with respect to microscopic and macroscopic information, respectively.
To better emphasize the role of macroscopic information in closed loop, this investigation is carried out under the following condition:

$$|g_{cl,i}(\tilde{\chi})| \leq \sum_{j=0}^{N} k_{ij}|\tilde{\chi}_j|. \tag{36}$$

where $\tilde{\chi} = \chi - \chi_e$ and $\tilde{\chi}_j = \chi_j - \chi_{e,j}$.

Because of the specific goal we target here, there is no interest in verifying SS. Therefore, we bypass the need to prove SS due to the result in Theorem 1 and focus on the possibility of ensuring ASS with a different technique than the one considered in Theorem 1. Since SS is ensured for each vehicle, by the converse Lyapunov theorem, there exists a function $W_i : \mathbb{R}^2 \to \mathbb{R}^+$ and constants $\underline{\alpha}, \bar{\alpha}, \alpha, \alpha' > 0$ such that

$$\underline{\alpha}|\tilde{\chi}_i|^2 \leq W_i(\tilde{\chi}_i) \leq \bar{\alpha}|\tilde{\chi}_i|^2 \tag{37}$$

$$\frac{\partial W_i(\tilde{\chi}_i)}{\partial \tilde{\chi}_i} f_{cl}(\tilde{\chi}_i) \leq -\alpha|\tilde{\chi}_i|^2 \tag{38}$$

$$\left|\frac{\partial W_i(\tilde{\chi}_i)}{\partial \tilde{\chi}_i}\right| \leq \alpha'|\tilde{\chi}_i| \tag{39}$$

By computing the time derivative of the Lyapunov function W_i with respect to the system with non-zero interconnected term, we obtain:

$$\begin{aligned}\dot{W}_i &= \frac{\partial W_i}{\partial \tilde{\chi}_i}(f_{cl}(\tilde{\chi}_i) + g_{cl,i}(\tilde{\chi})) \\ &\leq -\alpha|\tilde{\chi}_i|^2 + \left|\frac{\partial W_i}{\partial \tilde{\chi}_i}\right| |g_{cl,i}(\tilde{\chi}))| \\ &\leq -\alpha|\tilde{\chi}_i|^2 + \alpha'|\tilde{\chi}_i||g_{cl,i}(\tilde{\chi}_1, ..., \tilde{\chi}_N)|\end{aligned} \tag{40}$$

From (40), it is possible to remark how the constant values α and α' describe how the microscopic information described as norm of $\tilde{\chi}_i$ and the macroscopic one described by $g_{cl,i}(\tilde{\chi})$, respectively, impact on the system.

Proposition 1: In case of tailored macroscopic information $\psi_i(\rho) = g_{cl,i}(\chi)$ respecting condition (36), CAVs' mesoscopic controllers targeting ASS need to satisfy

$$k_{ii} < \frac{\alpha}{\alpha'} \ \forall \ i \in \{0, 1, \ldots, N\}, \tag{41}$$

where $k_{ii} > 0$ is the constant value considered in (36) describing the contribution of the macroscopic information of vehicle i on the predecessor follower system χ_i.

Proof 2: We focus on the possibility of ensuring ASS with similar arguments to the ones given in [7]. Let us consider the parameters $a_i > 0$ and define the composite function W_c:

$$W_c(\tilde{\chi}) = \sum_{i=0}^{N} a_i W_i(\tilde{\chi}_i) \tag{42}$$

that satisfies

$$\underline{\alpha}_c|\tilde{\chi}|^2 \leq W_c(\tilde{\chi}) \leq \bar{\alpha}_c|\tilde{\chi}|^2, \tag{43}$$

$$\underline{\alpha}_c = \min_{i \in \mathcal{I}_N^0}\{a_i\}\underline{\alpha}, \ \ \bar{\alpha}_c = \max_{i \in \mathcal{I}_N^0}\{a_i\}\bar{\alpha}. \tag{44}$$

The time derivative of the composite function in (42) is

$$\dot{W}_c(\tilde{\chi}) = \sum_{i=0}^{N} a_i \dot{W}_i(\tilde{\chi}_i) \tag{45}$$

By using (45) and (36), it results

$$\begin{aligned}\dot{W}_c(\tilde{\chi}) &\leq \sum_{i=0}^{N} a_i \left[-\alpha|\tilde{\chi}_i|^2 + \alpha'|\tilde{\chi}_i| \sum_{j=0}^{N} k_{ij}|\tilde{\chi}_j|\right] \\ &\leq \sum_{i=0}^{N} a_i \left[\left(-\alpha + \alpha' k_{ii}\right)|\tilde{\chi}_i|^2 + \alpha'|\tilde{\chi}_i| \sum_{j=0, j\neq i}^{N} k_{ij}|\tilde{\chi}_j|\right].\end{aligned} \tag{46}$$

It is worth noting that the two terms $-\alpha + \alpha' k_{ii}$ in (46) describe the contributions coming from the microscopic and the macroscopic information, respectively, for the stability analysis of the term $|\tilde{\chi}_i|^2$.

By defining the operator $\phi : \mathbb{R}^{2(N+1)} \to \mathbb{R}^{N+1}$ as

$$\phi(\tilde{\chi}) = [|\tilde{\chi}_0| \ |\tilde{\chi}_1| \ ... \ |\tilde{\chi}_N|]^T \tag{47}$$

then, equation (45) can be rewritten as

$$\dot{W}_c(\tilde{\chi}) \leq -\frac{1}{2}\phi(\tilde{\chi})^T Q \phi(\tilde{\chi}), \tag{48}$$

where the matrix Q is defined as

$$Q = \begin{bmatrix} z_0 & -a_1\alpha' k_{01} & \cdots & -a_n\alpha' k_{0N} \\ -a_0\alpha' k_{10} & z_1 & \cdots & -a_1\alpha' k_{1N} \\ \vdots & \vdots & \ddots & \vdots \\ -a_0\alpha' k_{N0} & -a_1\alpha' k_{N1} & \cdots & z_N \end{bmatrix} \tag{49}$$

with $z_i = 2a_i(\alpha - \alpha' k_{ii})$, $\forall i \in \{0, 1, \ldots, N\}$. The matrix Q can be written as

$$Q \doteq (DS + S^T D), \tag{50}$$

where

$$D = diag(a_0, a_1, ..., a_N) \tag{51}$$

and S is an $N + 1 \times N + 1$ matrix whose elements are

$$s_{ij} = \begin{cases} \alpha - \alpha' k_{ii}, & \text{if } i = j \\ -\alpha' k_{ij}, & \text{if } i < j \\ 0, & \text{if } i > j \end{cases} \tag{52}$$

According to [62, Lemma 9.7], in order to prove ASS using (48) a necessary condition is for S in (50) to be a $M-$matrix, such that $Q > 0$. Then, we must verify that each leading principal minor of S is positive. Therefore, a necessary condition for ASS is that

$$\alpha > \alpha' k_{ii} \ \forall \ i \in \{0, 1, \ldots, N\} \tag{53}$$

thus to satisfy condition (41). Then, by [62, Lemma 9.7] there exists a matrix D such that $Q > 0$. Consequently, $\dot{W}_c$ in (48) is negative definite. It follows that W_c in (42) is a Lyapunov function for the overall autonomous system ensuring ASS. ■

The condition stated in (41) is not required for the scenario explored in Section IV-B. This is because it stems from the condition (36), which is not a prerequisite for the theoretical analysis conducted in the case involving disturbances. However, we find it valuable to present this condition as it offers practical insights into how to balance the weight of microscopic information relative to macroscopic data in the mesoscopic controller. In essence, it emphasizes that the primary control focus should be on microscopic information while incorporating macroscopic data as an additional (but necessary) factor. The higher the value of α, the larger the allowed set of values for k_{ii}. On the contrary, the stronger the macroscopic contribution, the smaller the gain to take it into account. Therefore, under the realistic working hypothesis to consider gains $k_{ii} = k_{ij},\ \forall\ j \neq i \in \{0, 1, \ldots, N\}$, i.e., to weight the several tailored macroscopic contributions equally, condition (41) provides useful suggestions on how to weight the contribution of the microscopic and macroscopic information.

V. Simulations

We have conducted simulations using Python to validate the proposed approach rigorously. Due to space constraints, we refrain from displaying the complete array of cases detailed in the paper and instead focus on the most illustrative ones. As a result, we do not allocate a dedicated section to elucidate the case where the macroscopic information is shared at each macroscopic sampling time based on the aggregation process. Our emphasis is directed toward scenarios where the smart traffic manager seamlessly integrates the aggregation, estimation, and ARZ model simulation to furnish the necessary macroscopic data for the CAVs. Initially, it captures and processes microscopic data to compute the aggregation, employing these values as initial conditions for the ARZ model to generate and convey the required macroscopic information to the CAVs. It is important to note that aggregation occurs only at intervals of every fourth macroscopic sampling point. In the interim, the macroscopic data stems from the ARZ model simulation. Fig. 7 shows the suggested operating framework for the exchange of information. Even if less competitive in terms of performance, the considered framework is more realistic than a continuous share of information among the two levels of description of the traffic system, especially from the perspective of communication reduction targets. Clearly, the proposed method also offers the possibility to update the ARZ model at each macroscopic sampling time in a receding-horizon-like approach. Therefore, we consider two main situations:

a) exchange of tailored information for each CAV;
b) exchange of averaged information for the whole platoon.

We investigate a platoon of $N = 20$ CAVs with a desired inter-vehicular distance of $\Delta\bar{p} = 25\,\mathrm{m}$. The controller parameters are detailed in Table I. The microscopic control gains denoted as $K_{\Delta p}$ and $K_{\Delta v}$ are chosen to be similar to those used in a prior study [7]. It is worth noting that the theoretical conditions specified in (19) and (20), which depend on the values of $K_{\Delta p}$ and $K_{\Delta v}$, are empirically met in the simulations, although no formal computations are provided. Despite

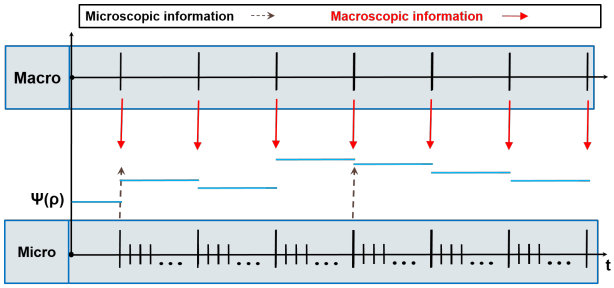

Fig. 7: The considered time scales and the exchange of information considered for simulations.

TABLE I: The values of the considered parameters.

Parameter	Value	Parameter	Value
$K_{\Delta p}$	1	$K_{\Delta v}$	2
$\Delta\bar{p}$	$25\,\mathrm{m}$	v_{ref}	$20\,\mathrm{m/s}$
$\mathbf{K^{m}}_{\rho}$	80	$\mathbf{K^{m}}_{v}$	0.1
dt_{ARZ}	$1\,\mathrm{s}$	dt_{ode}	$0.1\,\mathrm{s}$
ρ_{ref}	$\frac{1}{\Delta p_{ref}}$	v_{ref}	v_{ref}
V_{eq}	Greenshield model	Δp_{min}	$5\,\mathrm{m}$

the theoretical results are derived under unconstrained control inputs, we introduce constraints on accelerations in simulations for realism. Specifically, we set maximum acceleration and deceleration limits as $7m/s^2$ and $-7m/s^2$, respectively.

Simulations are carried out over a duration of 100 seconds, with a microscopic sampling time, denoted as dt_{ode}, set at $0.1\,\mathrm{s}$, and a macroscopic sampling time, denoted as dt_{ARZ}, set at $1\,\mathrm{s}$. While we do not furnish formal proofs of convergence for these particular sampling times, they are considered sufficiently small to be integrated into the modeling of the bounded disturbance. Nevertheless, it is essential to recognize that the absence of real-time updates impacts performance compared to the ideal scenario of instantaneous and frequent data transmission. More details on sampling conditions for DSS under mesoscopic approaches can be found in [64].

The initial inter-vehicle distances are randomly generated, while the initial speeds are uniform among all CAVs. The reference speed (v_{ref}) for the leader vehicle remains constant throughout the simulation. Each CAV is subject to a constant disturbance of $0.1\ m/s^2$ applied over the entire simulation duration. Additionally, between time instances $t = 20\,\mathrm{s}$ and $t = 25\,\mathrm{s}$, an additional constant disturbance with a magnitude of $1\ m/s^2$ influences the control inputs of each CAV. Furthermore, between $t = 35\,\mathrm{s}$ and $t = 60\,\mathrm{s}$, a sinusoidal disturbance affects the control inputs. A consistent color legend has been used for all figures. Each line in the figures corresponds to the trajectory of a predecessor-follower variable. The color scale employed ranges from a pink tint to cyan, indicating the position of the vehicles within the platoon, from the front (head vehicles) to the rear (tail vehicles).

A. Smart traffic manager implementation

We describe here how the smart traffic manager implements the algorithm in Section III. The results of the proposed implementation are communicated to the CAVs according to the chosen tailored or averaged information paradigm.

1) Microscopic information aggregation: At each macroscopic simulation time, the smooth particle hydrodynamics algorithm takes the CAVs' positions and speeds as parameters, as well as the desired space discretization step. For the sake of simplicity, this is considered equal to the desired distance. Moreover, it requires the knowledge of the minimum authorized distance to compute maximal density. It returns the vehicle density on a section road occupied by the platoon and the corresponding average velocity. The section road is delimited in front by the leader and back by the last follower.

The smoothing function $s_i(t)$ we consider is $s_i(t) = p_{i-1}(t) - p_i(t)$. To properly take into account the desired quantities, we consider $x \in D = [p_N, p_l]$, where p_N is the position of the last follower, and p_l is the leader's position at time t. We consider $\rho_{ref} = \frac{1}{\Delta p_{ref}} = \frac{1}{\Delta \bar{p}}$. The numerical values are depicted in Table I.

2) ARZ parameters estimation: The ARZ macroscopic model depends on some constant parameters and, in particular, on the density-speed equilibrium relationship (function $V(\rho)$ in equation (1)). To use this macroscopic model to derive our mesoscopic controller, we need to estimate these key parameters by following the methodology described in Algorithm 1. The training of the machine-learning algorithm (DNN) was done offline. Then, every time we send microscopic data to generate macroscopic data (aggregation process that occurs every fourth macroscopic sampling point), we run the neural network to update the estimation of the ARZ parameters.

3) Traffic flow emulation and ψ function: Once the previous steps are performed, the smart traffic manager implements simulations of the ARZ model using the computed initial conditions. It performs a simulation along four macroscopic sampling times (similarly to a prediction horizon of four steps) and provides the function ψ at each macroscopic sampling time to the CAVs. We consider a function ψ as

$$\psi = \mathbf{K}^{\mathbf{m}_\rho}(\rho_{ref} - \rho) + \mathbf{K}^{\mathbf{m}_\upsilon}(\upsilon_{ref} - \upsilon) \tag{54}$$

with $\mathbf{K}^{\mathbf{m}_\rho}$ and $\mathbf{K}^{\mathbf{m}_\upsilon}$ positive gains described in Table I, where the solutions for ρ and υ derived from the ARZ model in (1) exclusively pertain to the road segment occupied by the platoon. If the smart traffic manager aimed to maximize performance, it would perform aggregation and estimation at every macroscopic time step to update the ARZ model using a receding-horizon approach. However, this approach would necessitate significant information exchange and computational resources, which might not be feasible within the specified time constraints. In the following, we explore a scenario where the aggregation and estimation algorithms are executed only every fourth macroscopic sampling time to alleviate computational complexity.

B. Numerical results

As already mentioned, we consider two scenarios to show that the provided traffic manager succeeds in providing the macroscopic information that stabilizes the system.

1) Tailored information from the ARZ model: Fig. 8 and 9 depict the simulations in case of tailored information for each CAV, i.e., each CAV receives the specific dedicated value of $\psi_i(\rho)$.

In the initial phase, the vehicles swiftly converge to their target speeds and inter-vehicular distances. The deliberately chosen non-ideal initial conditions, coupled with the constraints on the control laws, result in an initial state that may appear disorderly. However, the trajectories of both inter-vehicular distance and speed errors remain within bounds during the transient period, which concludes in approximately 5 seconds (refer to Fig. 8). As demonstrated in Fig. 9, the high perturbation resulting from the initial conditions is effectively captured by the macroscopic function. This, in turn, causes the vehicles to follow a variable reference distance, resulting in a harmonious transient phase. Certainly, a shorter update horizon for the aggregate microscopic values, resulting in more frequent updates of macroscopic information, would have accelerated convergence. Nevertheless, the system demonstrates DSS even in scenarios where macroscopic updates lag behind the rapid changes occurring at the microscopic level.

The CAVs implementing the mesoscopic controller exhibit the ability to converge to the desired distances without significant perturbations, whether they are of constant magnitude, small or large, or sinusoidal. Despite the presence of these disturbances within the platoon, the sharing of macroscopic information ensures that the system maintains bounded trajectories. The efficacy of shock-wave mitigation is vividly illustrated in Fig. 8 and in the zooms therein, as the CAVs exhibit smoother dynamic behavior while traversing the platoon. Particularly noteworthy are the segments depicted in the zoomed sections around 20-25 seconds and 70-90 seconds. In these instances, it becomes evident how macroscopic information contributes to the smooth response of the follower vehicles in the face of added constant disturbances and effectively counteracts the effects of sinusoidal disturbances. Even though the macroscopic information is computed and shared every second, it proves to be sufficiently informative to ensure DSS. This is clearly exemplified in Fig. 9, which highlights the dependence of control inputs on this shared information. Indeed, the steady-state behavior exhibits both positive and negative peaks, which arise from both the disturbances affecting the system and the fluctuations in the considered macroscopic information.

We highlight the effective performance of the smart traffic manager. As depicted in Fig.9, it successfully computes both the aggregated values of ψ_i and those derived from the ARZ model. While these two sets of values are not identical, they exhibit a striking similarity. During the steady-state phase, the variation in ψ_i can be attributed to the aggregation of measured microscopic quantities. In contrast, the subsequent steps, where the value increases, correspond to the ARZ simulation and prediction of traffic flow. This observation underscores the capability of the smart traffic manager to manage both techniques efficiently. However, it clearly opens the room for better improvements.

2) Averaged information from the ARZ model: Fig. 10 and 11 depict the simulations in case of averaged information shared by the smart traffic manager to the whole set of CAVs, i.e., each CAV receives the same value of $\psi(\rho)$.

In a manner akin to the tailored scenario, the simulations demonstrate the effectiveness of the proposed approach in achieving the desired inter-vehicular distance and speed

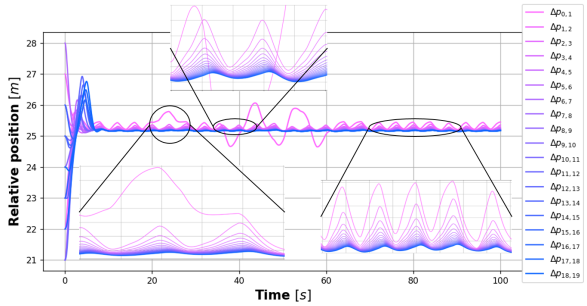

(a) Distances.

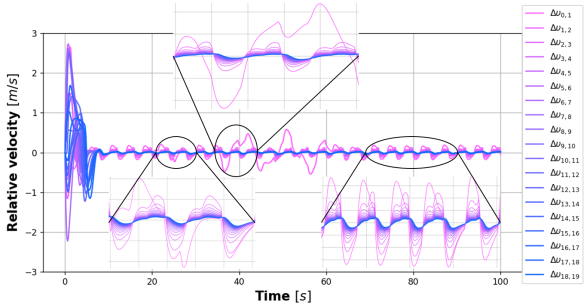

(b) Differences of speed.

Fig. 8: Tailored information case: (a) distances and (b) differences of speed of the platoon of 20 vehicles.

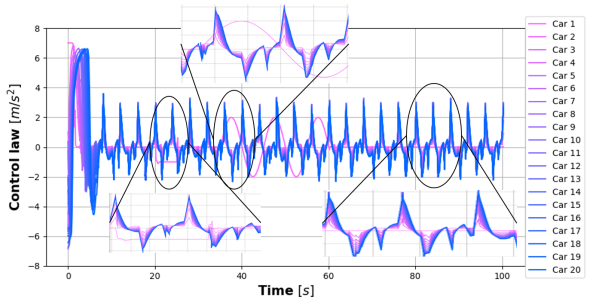

(a) Control inputs.

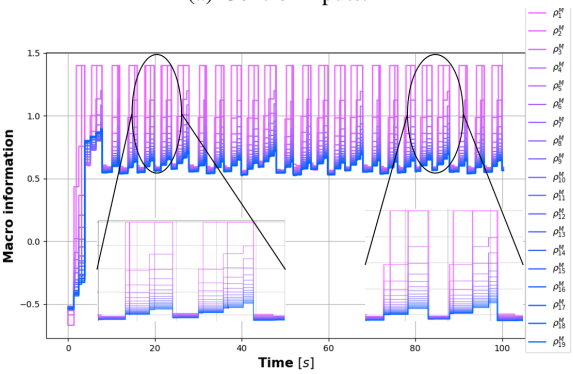

(b) Macroscopic function $\psi_i(\rho)$

Fig. 9: Tailored information case: (a) control inputs and (b) macroscopic information $\psi_i(\rho)$ of the platoon of 20 vehicles.

differential, as clearly illustrated in Fig. 10. However, the attenuation of disturbances is less pronounced. This is due to the uniform distribution of information to the entire set of vehicles, which subsequently acts directly on the control input, as outlined in (25). Nevertheless, the control inputs presented in Fig. (11) exhibit a behavior similar to those in Fig. (9). It is noteworthy that the magnitude of control efforts is less significant in the averaged case, as evidenced by comparing Fig. (11) to Fig. (9). This is attributed to the averaging behavior resulting from the sharing of a common variable rather than using tailored variables. Additionally, the macroscopic function $\psi(\rho)$, depicted in Fig. (11), exhibits a behavior akin to the one in Fig. (9). Indeed, both the tailored and averaged macroscopic information computed by the ARZ model (for the second, third, and fourth sampling of the macroscopic cycle) do not perfectly align with the value computed when aggregating microscopic information (for the first sampling). However, it is worth noting that the averaged quantity experiences fewer variations, and the predicted values are close to those obtained by aggregation in both cases. This suggests comparable performance for the smart traffic manager. Naturally, the error increases over the samplings, as one might expect, due to the greater distance from the real values. Nevertheless, thanks to an approach similar to the receding horizon method, the periodic aggregate measures help in keeping the error bounded.

The simulation outcomes illustrate that both the tailored and averaged functions empower CAVs to employ mesoscopic controllers effectively. This is achieved by leveraging the interplay between macroscopic and microscopic information, which helps alleviate stop-and-go waves while ensuring speed harmonization.

A notable concern that requires attention is the necessity for customizing the road segment and selecting appropriate neighbors for the computation of the average quantity. The proposed solution encounters challenges when dealing with small disturbances affecting a small road segment, as in the case of simulations, and the performance deteriorates as the size of the segment increases, despite the theoretical assurance of string stability. The issue emerges due to the limited influence and control over localized disturbances in the context of the segment's size. It is important to note that the approach considered here does not incorporate a macroscopic feedback mechanism that could modify microscopic values, such as speed references or maximum speeds. The alignment of microscopic values with optimal macroscopic ones might offer a potential solution to address this concern. Consequently, future research will place emphasis on exploring these aspects.

VI. Conclusion

The primary objective of this investigation was to establish a connection between microscopic and macroscopic traffic representations, ultimately incorporating macroscopic information into microscopic controllers to enhance overall traffic performance. The resulting mesoscopic controller has been formally verified to ensure disturbance string stability or string stability in scenarios without disturbances. As demonstrated throughout this paper and in simulations, this approach has a notably positive impact on mitigating stop-and-go patterns, reducing shock waves, and enhancing safety.

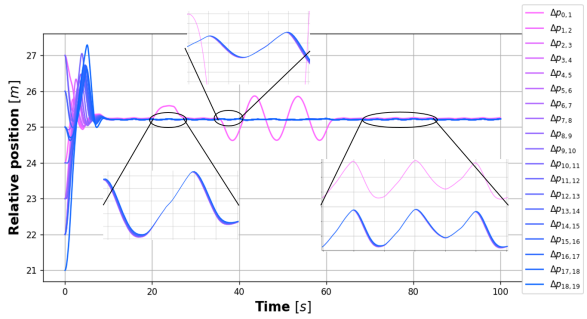

(a) Distances.

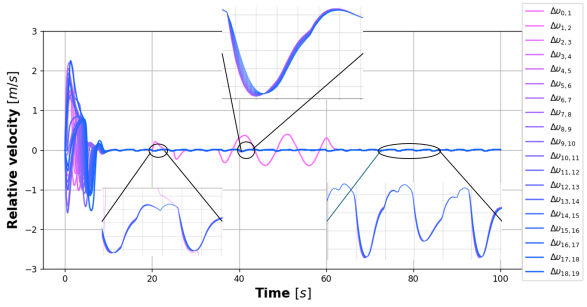

(b) Differences of speed.

Fig. 10: Averaged information case: (a) distances and (b) differences of speed of the platoon of 20 vehicles.

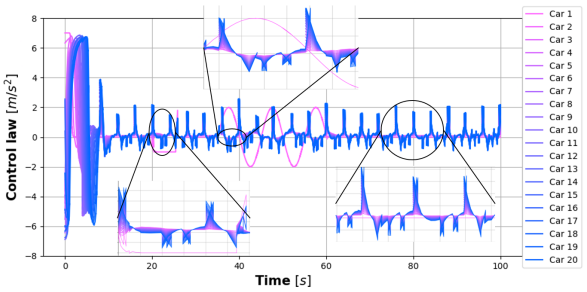

(a) Control inputs.

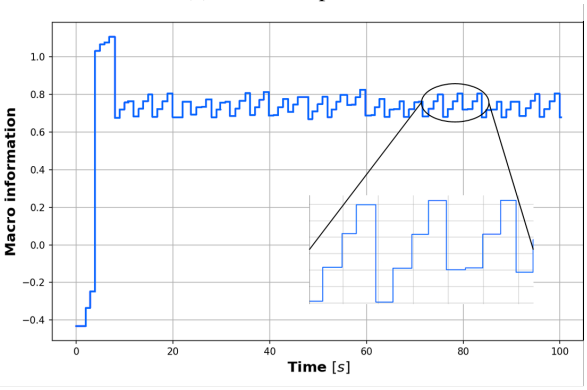

(b) Macroscopic function $\psi(\rho)$

Fig. 11: Averaged information case: (a) control inputs and macroscopic information $\psi(\rho)$ of the platoon of 20 vehicles.

The proposed smart traffic manager demonstrates the capability to compute macroscopic information through two phases: initial aggregation of macroscopic variables and subsequent real-time calculation from a realistic macroscopic model using a receding horizon approach. However, since this paper primarily focuses on the microscopic perspective and does not delve into macroscopic control, it outlines limitations related to potential equilibria. Future research will concentrate on closing the loop with a stabilizing macroscopic feedback system designed to align with desired macroscopic objectives, such as maximizing traffic throughput or achieving a specific average speed. Additionally, the study will explore mixed traffic scenarios involving both CAVs and human-driven vehicles sharing the road.

ACKNOWLEDGMENT

We would like to thank the anonymous Reviewers and the Associate Editor for taking the necessary time and effort to review the manuscript. We sincerely appreciate all your valuable comments and suggestions, which helped us in improving the quality of the manuscript.

REFERENCES

[1] Y. Du, M. A. Makridis, C. M. Tampère, A. Kouvelas, and W. Shang-Guan, "Adaptive control with moving actuators at motorway bottlenecks with connected and automated vehicles," *Transportation Research Part C: Emerging Technologies*, vol. 156, p. 104319, 2023.

[2] J. Guanetti, Y. Kim, and F. Borrelli, "Control of connected and automated vehicles: State of the art and future challenges," *Annual Reviews in Control*, vol. 45, pp. 18 – 40, 2018.

[3] A. Talebpour and H. S. Mahmassani, "Influence of connected and autonomous vehicles on traffic flow stability and throughput," *Transportation Research Part C: Emerging Technologies*, vol. 71, pp. 143 – 163, 2016.

[4] E. Uhlemann, "The US and Europe Advances V2V Deployment [Connected Vehicles]," *IEEE Vehicular Technology Magazine*, vol. 12, no. 2, pp. 18–22, June 2017.

[5] B. Besselink and K. H. Johansson, "String stability and a delay-based spacing policy for vehicle platoons subject to disturbances," *IEEE Transactions on Automatic Control*, vol. 62, no. 9, pp. 4376–4391, March 2017.

[6] S. Feng, Y. Zhang, S. E. Li, Z. Cao, H. X. Liu, and L. Li, "String stability for vehicular platoon control: Definitions and analysis methods," *Annual Reviews in Control*, vol. 47, pp. 81–97, March 2019.

[7] M. Mirabilio, A. Iovine, E. De Santis, M. D. Di Benedetto, and G. Pola, "String stability of a vehicular platoon with the use of macroscopic information," *IEEE Transactions on Intelligent Transportation Systems*, vol. 22, no. 9, pp. 5861–5873, 2021.

[8] ——, "Mesoscopic controller for string stability of platoons with disturbances," *IEEE Transactions on Control of Network Systems*, vol. 9, no. 4, pp. 1754–1766, 2022.

[9] M. Treiber and A. Kesting, *Traffic flows dynamics*. Springer, 2013.

[10] J. A. Rogge and D. Aeyels, "Vehicle platoons through ring coupling," *IEEE Transactions on Automatic Control*, vol. 53, no. 6, pp. 1370–1377, 2008.

[11] V. Giammarino, S. Baldi, P. Frasca, and M. Delle Monache, "Traffic flow on a ring with a single autonomous vehicle: An interconnected stability perspective," *IEEE Transactions On Intelligent Transportation Systems*, pp. 1–11, April 2020.

[12] T. G. Molnár, M. Hopka, D. Upadhyay, M. Van Nieuwstadt, and G. Orosz, *Virtual Rings on Highways: Traffic Control by Connected Automated Vehicles*. Cham: Springer International Publishing, 2023, pp. 441–479.

[13] M. K. Huan Yu, *Traffic Congestion Control by PDE Backstepping*. Birkhäuser Cham, 2022.

[14] D. Helbing, *Derivation of Non-local Macroscopic Traffic Equations and Consistent Traffic Pressures from Microscopic Car-Following Models*. Berlin, Heidelberg: Springer Berlin Heidelberg, 2013, pp. 247–269. [Online]. Available: https://doi.org/10.1007/978-3-642-32160-3_3

[15] G. Gunter, D. Gloudemans, R. E. Stern, S. McQuade, R. Bhadani, M. Bunting, M. L. Delle Monache, R. Lysecky, B. Seibold, J. Sprinkle, B. Piccoli, and D. B. Work, "Are commercially implemented adaptive

cruise control systems string stable?" *IEEE Transactions on Intelligent Transportation Systems*, vol. 22, no. 11, pp. 6992–7003, 2021.
[16] S. Fresca and A. Manzoni, "Pod-dl-rom: Enhancing deep learning-based reduced order models for nonlinear parametrized pdes by proper orthogonal decomposition," *Computer Methods in Applied Mechanics and Engineering*, vol. 388, p. 114181, 2022.
[17] D. Inzunza and P. Goatin, "A pinn approach for traffic state estimation and model calibration based on loop detector flow data," in *2023 8th International Conference on Models and Technologies for Intelligent Transportation Systems (MT-ITS)*, 2023, pp. 1–6.
[18] K. Binjaku, E. Meçe, C. Pasquale, and S. Sacone, "Control oriented freeway traffic modelling by physics-regularized machine learning," in *2023 IEEE 26th International Conference on Intelligent Transportation Systems (ITSC)*, 2023, pp. 6056–6061.
[19] J. Krook, M. Čičić, and K. H. Johansson, "Learning micro-macro models for traffic control using microscopic data," in *2022 European Control Conference (ECC)*, 2022, pp. 377–382.
[20] M. Garavello, P. Goatin, T. Liard, and B. Piccoli, "A multiscale model for traffic regulation via autonomous vehicles," *Journal of Differential Equations*, vol. 269, no. 7, pp. 6088–6124, 2020.
[21] M. Delle Monache and P. Goatin, "Scalar conservation laws with moving constraints arising in traffic flow modeling: An existence result," *Journal of Differential Equations*, vol. 257, no. 11, pp. 4015–4029, 2014.
[22] G. Piacentini, P. Goatin, and A. Ferrara, "A macroscopic model for platooning in highway traffic," *SIAM Journal on Applied Mathematics*, vol. 80, no. 1, pp. 639–656, 2020.
[23] A. Jamshidnejad, I. Papamichail, M. Papageorgiou, and B. De Schutter, "A mesoscopic integrated urban traffic flow-emission model," *Transportation Research Part C: Emerging Technologies*, vol. 75, pp. 45 – 83, 2017.
[24] A. Iovine, F. Valentini, E. De Santis, M. D. Di Benedetto, and M. Pratesi, "Safe human-inspired mesoscopic hybrid automaton for autonomous vehicles," *Nonlinear Analysis: Hybrid Systems*, vol. 25, pp. 192 – 210, 2017.
[25] A. Ibrahim, M. Čičić, D. Goswami, T. Basten, and K. Johansson, "Control of platooned vehicles in presence of traffic shock waves," *IEEE Intelligent Transportation Systems Conference (ITSC)*, pp. 1727–1734, 2019.
[26] D. Swaroop and R. Huandra, "Intelligent cruise control system design based on a traffic flow specification," *Vehicle System Dynamics: International Journal of Vehicle Mechanics and Mobility*, vol. 30, no. 5, pp. 319–344, November 1998.
[27] S. Darbha and K. Rajagopal, "Intelligent cruise control systems and traffic flow stability," *Transportation Research Part C: Emerging Technologies*, vol. 7, no. 6, pp. 329–352, 1999.
[28] H. Yu, J. Auriol, and M. Krstic, "Simultaneous downstream and upstream output-feedback stabilization of cascaded freeway traffic," *Automatica*, vol. 136, p. 110044, 2022.
[29] ——, "Output-feedback PDE control of traffic flow on cascaded freeway segments," *IFAC-PapersOnLine*, vol. 53, no. 2, pp. 7623–7628, 2020.
[30] A. Ferrara, G. P. Incremona, E. Birliba, and P. Goatin, "Multi-scale model-based hierarchical control of freeway traffic via platoons of connected and automated vehicles," *IEEE Open Journal of Intelligent Transportation Systems*, vol. 3, pp. 799–812, 2022.
[31] S. Hoogendoorn and P. Bovy, "State-of-the-art of vehicular traffic flow modeling," *J. Syst. Cont. Eng.*, vol. 215, pp. 283–303, 06 2001.
[32] M. Lighthill and G. Whitham, "On kinematic waves ii. a theory of traffic flow on long crowded roads," *Proceedings of the Royal Society of London. Series A. Mathematical and Physical Sciences*, vol. 229, no. 1178, pp. 317–345, 1955.
[33] P. Richards, "Shock waves on the highway," *Operations research*, vol. 4, no. 1, pp. 42–51, 1956.
[34] A. Aw and M. Rascle, "Resurrection of "second order" models of traffic flow," *SIAM Journal on Applied Mathematics*, vol. 60, no. 3, pp. 916–938, 2000.
[35] H. Zhang, "A non-equilibrium traffic model devoid of gas-like behavior," *Transportation Research Part B: Methodological*, vol. 36, no. 3, pp. 275–290, 2002.
[36] M. Flynn, A. Kasimov, J. Nave, R. Rosales, and B. Seibold, "Self-sustained nonlinear waves in traffic flow," *Physical Review E*, vol. 79(5), no. 1, pp. 56–113, 2009.
[37] M. Garavello and B. Piccoli, "Traffic flow on a road network using the Aw–Rascle model," *Communications in Partial Differential Equations*, vol. 31, no. 2, pp. 243–275, 2006.
[38] M. Herty and M. Rascle, "Coupling conditions for a class of second-order models for traffic flow," *SIAM Journal on mathematical analysis*, vol. 38, no. 2, pp. 595–616, 2006.
[39] S. Siri, C. Pasquale, S. Sacone, and A. Ferrara, "Freeway traffic control: A survey," *Automatica*, vol. 130, p. 109655, 2021.
[40] G. Bastin and J.-M. Coron, *Stability and boundary stabilization of 1-D hyperbolic systems*. Springer, 2016, vol. 88.
[41] I. Karafyllis and M. Papageorgiou, "Feedback control of scalar conservation laws with application to density control in freeways by means of variable speed limits," *Automatica*, vol. 105, pp. 228–236, 2019.
[42] H. Yu and M. Krstic, "Traffic congestion control for Aw-Rascle-Zhang model," *Automatica*, vol. 100, pp. 38–51, 2019.
[43] L. Zhang, C. Prieur, and J. Qiao, "PI boundary control of linear hyperbolic balance laws with stabilization of ARZ traffic flow models," *Systems & Control Letters*, vol. 123, pp. 85–91, 2019.
[44] N. Espitia, J. Auriol, H. Yu, and M. Krstic, "Traffic flow control on cascaded roads by event-triggered output feedback," *International Journal of Robust and Nonlinear Control*, vol. 32, no. 10, pp. 5919–5949, 2022.
[45] P. Lax and B. Wendroff, "Systems of conservation laws," 11 1958. [Online]. Available: https://www.osti.gov/biblio/4244712
[46] W. Levine and M. Athans, "On the optimal error regulation of a string of moving vehicles," *IEEE Transactions on Automatic Control*, vol. 11, no. 3, pp. 355–361, 1966.
[47] L. Peppard, "String stability of relative-motion pid vehicle control systems," *IEEE Transactions on Automatic Control*, vol. 19, no. 5, pp. 579–581, 1974.
[48] T. Nagatani, "Traffic jams induced by fluctuation of a leading car," *Physical Review E*, vol. 61, no. 4, p. 3534, 2000.
[49] C.-C. Chien, Y. Zhang, and P. A. Ioannou, "Traffic density control for automated highway systems," *Automatica*, vol. 33, no. 7, pp. 1273–1285, 1997.
[50] D. Swaroop and J. K. Hedrick, "String stability of interconnected systems," *IEEE Transactions on Automatic Control*, vol. 41, no. 3, pp. 349–357, Mar 1996.
[51] G. Piacentini, M. Čičić, A. Ferrara, and K. H. Johansson, "VACS equipped vehicles for congestion dissipation in multi-class CTM framework," in *2019 18th European Control Conference (ECC)*, June 2019, pp. 2203–2208.
[52] L. Xiao and F. Gao, "Practical string stability of platoon of adaptive cruise control vehicles," *IEEE Transactions on Intelligent Transportation Systems*, vol. 12, no. 4, pp. 1184–1194, Dec 2011.
[53] M. di Bernardo, A. Salvi, and S. Santini, "Distributed consensus strategy for platooning of vehicles in the presence of time-varying heterogeneous communication delays," *IEEE Transactions on Intelligent Transportation Systems*, vol. 16, no. 1, pp. 102–112, 2015.
[54] J. Ploeg, N. van de Wouw, and H. Nijmeijer, "$\mathcal{L}_p$ string stability of cascaded systems application to vehicle platooning," *IEEE Transactions on Control Systems Technology*, vol. 22, no. 2, pp. 786–793, March 2014.
[55] Y. Zheng, S. Ebel Li, K. Li, F. Borrelli, and J. Hedrick, "Distributed model predictive control for heterogeneous vehicle platoons under unidirectional topologies," *IEEE Transactions on Control Systems Technology*, vol. 25, no. 3, pp. 899–910, May 2017.
[56] F. A. Chiarello and A. Tosin, "Macroscopic limits of non-local kinetic descriptions of vehicular traffic," *Kinetic and Related Models*, vol. 16, no. 4, pp. 540–564, 2023.
[57] J. Auriol, N. Kazemi, and S.-I. Niculescu, "Sensing and computational frameworks for improving drill-string dynamics estimation," *Mechanical Systems and Signal Processing*, vol. 160, p. 107836, 2021.
[58] J. Auriol, R. Shor, S.-I. Niculescu, and N. Kazemi, "Estimating drill string friction with model-based and data-driven methods," in *2022 American Control Conference (ACC)*. IEEE, 2022, pp. 3464–3469.
[59] R. N. Bracewell, *The Fourier Transform and Its Applications*, 3rd ed. McGraw-Hill Science/Engineering/Math, 2000.
[60] R. C. Gonzalez and R. E. Woods, *Digital Image Processing*, 4th ed. Pearson, 2018.
[61] A. Ferrara, S. Sacone, and S. Siri, *Microscopic and Mesoscopic Traffic Models*. Cham: Springer International Publishing, 2018, pp. 113–143. [Online]. Available: https://doi.org/10.1007/978-3-319-75961-6_5
[62] H. K. Khalil, *Nonlinear systems*. Prentice Hall, 2002.
[63] M. Mirabilio, A. Iovine, E. De Santis, M. D. Di Benedetto, and G. Pola, "Scalable mesh stability of nonlinear interconnected systems," *IEEE Control Systems Letters*, vol. 6, pp. 968–973, 2022.
[64] A. Iovine, M. Mattioni, and G. Tedeschi, "Sampled-data string stability for a platoon of heterogeneous vehicles via a mesoscopic approach," in *2024 European Control Conference (ECC)*, 2024, pp. 3364–3369.

Lea Prade Njoua Dongmo Lea Prade Njoua Dongmo received the B.S. in fundamental mathematics and computer science in 2017 from the University of Dschang, Cameroon. She additionally received the B.S. and M.S. degrees in computer science and automation engineering from the University of Parma, Emilia-Romagna, Italy, in 2021 and 2024, respectively, and a double degree M.S. in control, image and signal processing from Paris-Saclay University in 2024. Now she is working as Control System engineer at Ampere (Renault), Renault research Headquarter located in GUYANCOURT, France.

Her research interests focus on identification and control of complex systems.

Jean Auriol received his Master degree in civil engineering in 2015 (major: applied maths) in MINES ParisTech, part of PSL Research University and in 2018 his Ph.D. degree in control theory and applied mathematics from the same university (Centre Automatique et Systèmes). His Ph.D. thesis, titled Robust design of backstepping controllers for systems of linear hyperbolic PDEs, has been nominated for the best thesis award given by the GDR MACS and the Section Automatique du Club EEA in France. From 2018 to 2019, he was a Postdoctoral Researcher at the Department of Petroleum Engineering, University of Calgary, AB, Canada, where he was working on the implementation of backstepping control laws for the attenuation of mechanical vibrations in drilling systems. From December 2019, he is a Researcher (Chargé de Recherches) at CNRS, Université Paris-Saclay, Centrale Supelec, Laboratoire des Signaux et Systèmes (L2S), Gif-sur-Yvette, France. His research interests include robust control of hyperbolic systems, neutral systems, networks, and interconnected systems

Alessio Iovine Alessio Iovine (M'18) received the B.Sc. and M.Sc. degrees in electrical engineering and computer science from the University of L'Aquila, L'Aquila, Italy, in 2010 and 2012, respectively, and the European Doctorate degree in information science and engineering in 2016 from the University of L'Aquila, L'Aquila, Italy, in collaboration with CentraleSupélec, Paris-Saclay University, Gif-sur-Yvette, France. From 2016 to 2020, he held Post-Doctoral positions at University of L'Aquila, Efficacity Research Center (France), University of California at Berkeley (USA), and CentraleSupélec. In 2020, he joined the CNRS as Researcher and is with the L2S, Paris-Saclay University.

Dr. Iovine has co-authored more than 50 papers covering advanced control methods for power and energy systems as well as traffic control ones, with smart grids and autonomous vehicles as core applications. He is a member of the IFAC Technical Committee TC 6.3 Power and Energy Systems since 2020.

His research interests focus on control methods for cyber-physical systems, particularly in the modeling and control of large-scale systems and optimal multi-level information management. Recently, he has concentrated on developing optimal control strategies to improve the integration and utilization of renewables and storage devices in power systems, as well as reducing consumption and maximizing traffic throughput in cooperative intelligent transportation systems.